

Simpler is better: A comparative study of randomized algorithms for computing the CUR decomposition

Yijun Dong and Per-Gunnar Martinsson

The University of Texas at Austin

May 31, 2022

Abstract

The CUR decomposition is a technique for low-rank approximation that selects small subsets of the columns and rows of a given matrix to use as bases for its column and row spaces. It has recently attracted much interest, as it has several advantages over traditional low rank decompositions based on orthonormal bases. These include the preservation of properties such as sparsity or non-negativity, the ability to interpret data, and reduced storage requirements. The problem of finding the skeleton sets that minimize the norm of the residual error is known to be NP-hard, but classical pivoting schemes such as column pivoted QR work tend to work well in practice. When combined with randomized dimension reduction techniques, classical pivoting based methods become particularly effective, and have proven capable of very rapidly computing approximate CUR decompositions of large, potentially sparse, matrices. Another class of popular algorithms for computing CUR decompositions are based on drawing the columns and rows randomly from the full index sets, using specialized probability distributions based on leverage scores. Such sampling based techniques are particularly appealing for very large scale problems, and are well supported by theoretical performance guarantees. This manuscript provides a comparative study of the various randomized algorithms for computing CUR decompositions that have recently been proposed. Additionally, it proposes some modifications and simplifications to the existing algorithms that leads to faster execution times.

1 Introduction

The CUR decomposition selects small subsets of skeleton rows and columns that preserve the spectral properties of the original matrix well. Let $\mathbf{A} \in \mathbb{R}^{m \times n}$ be a given matrix whose singular values decay fast enough that low rank approximation is a reasonable objective. We then aim to select the sets of row skeletons $I \subseteq [m]$ and column skeletons $J \subseteq [n]$ of sizes $|I| < m$ and $|J| < n$ such that for $\mathbf{C} := \mathbf{A}(:, J)$, $\mathbf{R} := \mathbf{A}(I, :)$, and some small middle matrix \mathbf{U} , the CUR decomposition

$$\tilde{\mathbf{A}}_{m \times n} := \mathbf{C}_{m \times |I|} \mathbf{U}_{|I| \times |J|} \mathbf{R}_{|J| \times n} \quad (1)$$

is such that $\|\mathbf{A} - \tilde{\mathbf{A}}\|$ is reasonably close to minimal. We will focus on approximation in either the spectral or the Frobenius norm.

Comparing to classical low-rank factorizations with orthogonal basis vectors such as the singular value decomposition (SVD), the CUR decomposition has the advantage of preserving the sparsity and interpretability of the original data. Nevertheless, in contrast to the SVD that is known for providing the optimal low-rank approximation, the CUR decomposition suffers from weaker guarantees on the spectrum recovery for an arbitrary matrix \mathbf{A} . In general, the CUR

decomposition preserves the leading spectrum reasonably well for \mathbf{A} with rapid spectral decay, while it tends to give a far-from-optimal low-rank approximation for \mathbf{A} with a flat spectrum.

Numerous algorithms have been proposed to select the skeleton rows and columns for the CUR decomposition. Two common categories of CUR algorithms are the greedy skeleton selection based on pivoting, and the random skeleton selection based on sampling. The sampling based CUR decomposition consists of delicately constructing weighted distributions over the columns and rows of \mathbf{A} that reflect their relative importance in preserving the spectrum, as well as a sampling scheme from which the row and column skeleton sets are drawn. Some well-known importance sampling schemes for the CUR decomposition include the leverage score sampling [11], [14], and the optimal CUR matrix decomposition [19]. The sampling based CUR decomposition induces a wide range of theoretical works. For instance, the recent results [32] unveil the connection between the leverage score sampling and the determinantal stochastic point process (DPP), a type of stochastic point processes with distributions characterized by the determinants of principal minors in a kernel matrix that enjoys certain sense of optimality in expectation for the Nyström method.

Alternatively, the CUR skeletons can be selected greedily with classical pivoting schemes in linear algebra such as the column pivoted QR [27]. Although the classical pivoting procedures may be inefficient or infeasible for large-scale problems, these procedures can easily be coupled with randomized subspace embeddings for more favorable efficiency without noticeably compromising the accuracy [27]. This gives rise to a class of pivoting based randomized CUR decomposition algorithms, including the CUR-ID [27] and the DEIM induced CUR decomposition [23]. This manuscript aims to provide a brief overview for some common pivoting based randomized CUR algorithms, and then propose some modifications and simplifications that improve performance.

For the sake of simplicity, we assume that \mathbf{A} admits a good rank- k approximation with a known rank $k \ll \min(m, n)$ ¹, and we aim to find column and row skeleton sets of size k that come close to minimizing $\|\mathbf{A} - \mathbf{CUR}\|_\xi$, where ξ indicates either the spectral ($\xi = 2$) or the Frobenius ($\xi = F$) norm. The pivoting based randomized CUR decompositions can be partitioned into two stages.

1. The first stage involves the randomized construction of a rank- k approximation of \mathbf{A} , denoted as $\widehat{\mathbf{A}}_k$.
2. The second stage is the greedy skeleton selections by applying the classical pivoting schemes to the low-dimensional representation $\widehat{\mathbf{A}}_k$.

The CUR decomposition is closely related to the column subset selection problem (CSSP) and the interpolative decomposition (ID), both of which aim to select a set of skeleton columns $\mathbf{C} = \mathbf{A}(:, J)$ for some $J \subseteq [n]$ such that $\|\mathbf{A} - \mathbf{CC}^\dagger \mathbf{A}\|_\xi$ ² is close to the minimal. In particular, to select a skeleton set from the n columns of \mathbf{A} , we replace the rank- k approximation $\widehat{\mathbf{A}}_k$ in the above two-stage scheme with a small sample matrix of the row space, \mathbf{X} , which contains n columns such that $\mathbf{AX}^\dagger \mathbf{X} \approx \mathbf{A}$. Following by applying the classical pivoting schemes to \mathbf{X} in the second stage, we have a randomized greedy procedure for the CSSP and the ID [27]. Meanwhile, with an oracle for the CSSP or the ID, the CUR decomposition can be computed either by evaluating the CSSP or the ID for both the column and the row spaces of \mathbf{A} simultaneously, or by first selecting the skeletons on one side and sequentially determining the skeletons on the other side by applying the oracle on the selected skeletons.

The manuscript is organized as follows: In Section 2, we start with an overview of some common subspace embeddings for constructing low-rank sketches and approximating low-rank decom-

¹For \mathbf{A} that is numerically low rank or with a fast decaying spectrum, this assumption can be relaxed by determining the proper rank adaptively with respect to a given tolerance $\|\mathbf{A} - \mathbf{CUR}\|_\xi \leq \tau \cdot \text{OPT}$ where OPT denotes the optimal rank- k approximation error.

² \dagger denotes the Moore–Penrose pseudo-inverse of the matrix.

positions of \mathbf{A} . In Section 3, we discuss some randomized greedy column selection algorithms with pivoting that provides solutions for the CSSP and the ID. Then in Section 4, we extend these pivoting based randomized skeleton selection procedures to the construction of CUR decompositions. In Section 5, we briefly discuss the skeleton selection in the single-view setting where the original matrix \mathbf{A} can be visited only once, and the order in which entries are viewed cannot be specified.

2 Sketching of the Column Space

We start with the first stage in the pivoting based randomized CUR decompositions, namely, the construction of a sketch or low-rank decomposition of $\mathbf{A} \in \mathbb{R}^{m \times n}$ with the randomized subspace embeddings. Without loss of generality, we assume in this section that $m \geq n$. Then for the sake of efficiency, the first stage initiates with the sketching of the column space.

2.1 Subspace Embeddings

The subspace embedding is a linear map that compresses the high dimensional data to a lower dimension, while preserving the distance among the data points. To be specific, given an error parameter $\epsilon > 0$ and a probability parameter $0 < \delta < 1$, an (ϵ, δ) -oblivious l_2 -subspace embedding is a distribution \mathcal{S} with support over a family of linear maps $\text{supp}(\mathcal{S}) \subseteq \{\mathbf{S} \in \mathbb{R}^{k \times m} : \mathbf{S} : \mathbb{R}^m \rightarrow \mathbb{R}^k\}$ such that, for an ϵ -subspace embedding $\mathbf{S} \sim \mathcal{S}$, with probability at least $1 - \delta$,

$$(1 - \epsilon) \|\mathbf{A}\mathbf{x}\|_2^2 \leq \|\mathbf{S}\mathbf{A}\mathbf{x}\|_2^2 \leq (1 + \epsilon) \|\mathbf{A}\mathbf{x}\|_2^2, \quad \forall \mathbf{A} \in \mathbb{R}^{m \times n}, \mathbf{x} \in \mathbb{R}^n. \quad (2)$$

Depending on the distribution \mathcal{S} , the lower bound on the embedding dimension k , in order to fulfill (2), is a function of m , n , ϵ , and δ .

The randomized subspace embedding has close relation to the Johnson-Lindenstrauss transform and the restricted isometry property, and is studied in a wide scope of literature [7], [9], [12], [17], [18], [20], [21], [25], [31], etc.. Some popular choices of the oblivious l_2 -subspace embedding include the Gaussian random matrices [6], [12], [20], [31], subsampled randomized trigonometric transforms [8], [9], [12], [13], [15], [31], and sparse sign matrices [17], [18], [20], [25], [26], [31].

Gaussian random matrix The Gaussian random matrix provides a straightforward oblivious l_2 -subspace embedding. A Gaussian embedding matrix $\mathbf{S} \in \mathbb{R}^{k \times m}$ contains entries drawn i.i.d. from a Gaussian distribution, $S_{ij} \sim \mathcal{N}(\mu, \sigma^2)$. As discussed extensively in [6], [12], [20], [31], the scaled zero-mean Gaussian embedding matrix $\mathbf{S} \in \mathbb{R}^{k \times m}$ with $S_{ij} \sim \mathcal{N}(0, 1/k)$ i.i.d. provides an oblivious (ϵ, δ) - l_2 -subspace embedding for any $\mathbf{A} \in \mathbb{R}^{m \times n}$ when

$$k = \Theta\left(\frac{1}{\epsilon^2} \left(n + \log\left(\frac{1}{\delta}\right)\right)\right). \quad (3)$$

The storage of a Gaussian embedding map takes $O(km)$ floats, and the sketching complexity of the Gaussian embedding is $O(nnz(\mathbf{A})k)$ ³.

Subsampled randomized trigonometric transform The subsampled randomized trigonometric transform (SRTT) is a family of structured non-Gaussian embeddings that shows comparable embedding performance as the Gaussian embeddings [31]. The subsampled randomized

³ $nnz(\mathbf{A})$ stands for the number of nonzero elements in the matrix \mathbf{A} .

Fourier transforms (SRFT) is a common choice among the SRTTs for subspace embedding [12], and can be represented as a matrix $\mathbf{S} \in \mathbb{C}^{k \times m}$ such that

$$\mathbf{S} = \sqrt{\frac{m}{k}} \mathbf{P} \mathbf{F} \mathbf{D}, \quad (4)$$

where $\mathbf{P} \in \mathbb{R}^{k \times m}$ consists of k rows of a random $m \times m$ permutation matrix, corresponding to k out of the m coordinates sampled uniformly at random. $\mathbf{F} \in \mathbb{C}^{m \times m}$ represents the unitary discrete Fourier transform (DFT) such that for $p, q \in [m]$,

$$\mathbf{F}_{pq} = \frac{1}{\sqrt{m}} \cdot e^{-2\pi i \frac{(p-1)(q-1)}{m}}.$$

$\mathbf{D} \in \mathbb{R}^{m \times m}$ is a diagonal matrix such that for each $i \in [m]$, D_{ii} is sampled uniformly and independently from the complex unit circle.

Storing an SRFT map takes $O(m \log m)$ complex numbers. The column sketch $\mathbf{S} \mathbf{A} \in \mathbb{C}^{k \times n}$ can be constructed with $O(mn \log k)$ operations via the subsampled fast Fourier transform [9], [12], [31]. For a slightly larger lower bound on the embedding dimension than that of the Gaussian embedding,

$$k = \Omega\left(\frac{1}{\epsilon^2}(\log n)\left(\sqrt{n} + \sqrt{\log m}\right)^2\right), \quad (5)$$

the SRFT gives an oblivious $(\epsilon, 0.01)$ - l_2 -subspace embedding [20], [31]. The lower bound (5) for the SRFT is larger than that required by the Gaussian embedding (3), by a factor of $O(\log n)$. Indeed, [12] (Section 11) instantiates that this $O(\log n)$ factor is inevitable in the worse case, with a contrived matrix, leveraging the idea of the coupon collector. Nevertheless, the SRFT usually exhibits similar empirical performance as the Gaussian embedding in numerous applications [12], [31].

Sparse subspace embedding The subspace embedding is commonly applied to large-scale sparse systems for dimension reduction. However, neither the Gaussian embeddings nor the SRFT preserves the sparsity of the input matrix. As an alternative, the sparse subspace embedding is a class of non-Gaussian oblivious subspace embeddings that exploits the sparsity of the input.

The CountSketch matrix is an intuitive choice for sparse subspace embedding. As introduced in [25], given a k -wise independent hash function $h : [m] \rightarrow [k]$ (e.g., for all $i \in [m]$, draw $h(i)$ from $[k]$ uniformly and independently), a CountSketch matrix $\mathbf{S} \in \mathbb{R}^{k \times m}$ ($k \leq m$) is defined such that for all $i \in [m]$,

$$S_{ji} = \begin{cases} Z_i & j = h(i) \\ 0 & \text{otherwise} \end{cases}, \quad (6)$$

where Z_i are i.i.d. random variables with Rademacher distribution (i.e., $\Pr[Z_i = 1] = \Pr[Z_i = -1] = 1/2$). Despite the favorable $O(m \log k)$ memory cost and $O(nnz(\mathbf{A}))$ computational cost, the CountSketch matrix requires $k \geq O(n^2/\delta\epsilon^2)$ to guarantee the ϵ -distortion with probability at least $1 - \delta$ ([17], [18], [20]). The prohibitive $O(n^2)$ dependence compromises the practical advantage of the CountSketch matrix for subspace embedding.

The sparse sign matrix is a variation of the CountSketch matrix that enjoys a more practical lower bound on k . For a fixed sparsity parameter $2 \leq \zeta \leq k$, the sparse sign matrix, $\mathbf{S} \in \mathbb{R}^{k \times m}$ takes the form,

$$\mathbf{S} = \sqrt{\frac{1}{\zeta}} \begin{bmatrix} \mathbf{s}_1 & \mathbf{s}_2 & \dots & \mathbf{s}_m \end{bmatrix}, \quad (7)$$

where $\mathbf{s}_j \in \mathbb{R}^k$ are i.i.d. random vectors such that for each $j \in [m]$, \mathbf{s}_j has exactly ζ nonzero entries in uniformly random coordinates, and each nonzero entry is drawn from the Rademacher distribution. A sparse sign matrix takes $O(\zeta m \log k)$ floats to store, and can be applied to an $m \times n$ matrix \mathbf{A} with $O(\text{nnz}(\mathbf{A})\zeta)$ operations. The sparse sign matrix can be approximated as a scaled sum of a set of CountSketch matrices. The subtlety is that, since the number of non-zeros in each column is fixed, such a set of CountSketch matrices will have to be dependent. [21], [31] demonstrates that, for fixed $B > 2$, $\delta < 1/2$, $\epsilon < 1/2$, a sparse sign matrix $\mathbf{S} \in \mathbb{R}^{k \times m}$ with

$$k = O\left(\frac{1}{\epsilon^2} B n \log\left(\frac{n}{\delta}\right)\right), \quad \zeta = O\left(\frac{1}{\epsilon} \log_B\left(\frac{n}{\delta}\right)\right). \quad (8)$$

gives an oblivious (ϵ, δ) - l_2 -subspace embedding. The lower bound (8) for the sparse sign matrix is also greater than that of the Gaussian embedding (3) by a factor of $O(\log n)$. However empirically, [26], [31] suggests that a constant sparsity parameter $\zeta = \min(k, 8)$ is usually sufficient for the sparse sign matrix to achieve as competitive performance as the Gaussian embedding and the SRFT.

We summarize the asymptotic complexities, denoted as $T_s(k, \mathbf{A})$, of applying the above oblivious l_2 -subspace embeddings $\mathbf{S} \in \mathbb{R}^{k \times m}$ to a matrix $\mathbf{A} \in \mathbb{R}^{m \times n}$ in Table 1.

Subspace embedding	Complexity
Gaussian embedding	$O(\text{nnz}(\mathbf{A})k)$
SRFT	$O(mn \log k)$
Sparse sign matrix	$O(\text{nnz}(\mathbf{A})\zeta)$, $\zeta = \min(k, 8)$

Table 1: The asymptotic complexities of applying an oblivious l_2 -subspace embedding $\mathbf{S} \in \mathbb{R}^{k \times m}$ to a matrix $\mathbf{A} \in \mathbb{R}^{m \times n}$, denoted as $T_s(k, \mathbf{A})$.

2.2 Low-rank Approximations and Power Iterations

Leveraging ⁴ the above subspace embeddings, we can construct the linear sketches and various low-rank decompositions accordingly. To start with, we introduce some notations, and establish the optimal rank- k approximation error.

Throughout this survey, we consider a fixed matrix $\mathbf{A} \in \mathbb{R}^{m \times n}$ with rank $r \leq \min(m, n)$. For an arbitrary k with $1 \leq k \leq r$, we denote the best rank- k approximation of \mathbf{A} given by the singular value decomposition (SVD) [1] as \mathbf{A}_k such that,

$$\|\mathbf{A} - \mathbf{A}_k\| = \sigma_{k+1}(\mathbf{A}), \quad \|\mathbf{A} - \mathbf{A}_k\|_F = \left(\sum_{i=k+1}^r \sigma_i^2(\mathbf{A})\right)^{\frac{1}{2}}, \quad (9)$$

where $\sigma_i(\mathbf{A})$ denotes the i -th largest singular value of \mathbf{A} , respectively. To simplify the demonstration, we assume a known target rank $k \ll \min(m, n)$ such that \mathbf{A} admits a good rank- l approximation $\widehat{\mathbf{A}}_l$ with $\|\mathbf{A} - \widehat{\mathbf{A}}_l\|_\xi \leq \tau \|\mathbf{A} - \mathbf{A}_k\|_\xi$ where $\xi = 2$ or F , $\tau > 0$ is a small tolerance, and $l \geq k$ is the true decomposition rank with oversampling. Furthermore, we denote \tilde{l} as the embedding dimension, or the sample size, of the subspace embedding $\mathbf{S} : \mathbb{R}^m \rightarrow \mathbb{R}^{\tilde{l}}$ such that $\tilde{l} \geq l \geq k$ and $l \leq r$. In specific, $\tilde{l} > l$ when the subspace embedding \mathbf{S} results in a rank-deficient

⁴This section is a bit too detailed, given that it is background. It is fine for the arxiv version, but before we submit to a journal, we should tighten this one up.

sketch $\mathbf{SA} \in \mathbb{R}^{\tilde{l} \times n}$ with $\text{rank}(\mathbf{SA}) = l$. If we further assume that $\tilde{l} \ll r$ (which is a reasonable assumption for the matrices that admit low-rank approximations), then $\tilde{l} = l$ with high probability [12], [31].

With an oblivious subspace embedding $\mathbf{S} \in \mathbb{R}^{\tilde{l} \times m}$, the sketch of the column space $\mathbf{X} = \mathbf{SA}$ characterizes a rank- l projector $\mathcal{P}_X = \mathbf{X}^\dagger \mathbf{X} \in \mathbb{R}^{n \times n}$ that defines the corresponding rank- l approximation,

$$\widehat{\mathbf{A}}_l = \mathbf{A} \mathcal{P}_X = \mathbf{A} \mathbf{X}^\dagger \mathbf{X} \quad (10)$$

In terms of the theory, [12], [31] provides a set of expectation and probabilistic error bounds, in both the spectral and the Frobenius norms, for the rank- l approximation error.

Lemma 2.1 ([12], Theorem 10.5-10.9). *With a Gaussian embedding $\mathbf{\Gamma} \in \mathbb{R}^{l \times m}$ such that $k+4 \leq l \leq r$, and the column sketch $\mathbf{X} = \mathbf{\Gamma} \mathbf{A}$ satisfies that, in expectation,*

$$\mathbb{E} \left\| \mathbf{A} (\mathbf{I} - \mathbf{X}^\dagger \mathbf{X}) \right\|_F \leq \sqrt{\frac{l-1}{l-k-1}} \left(\sum_{j \geq k+1} \sigma_j(\mathbf{A})^2 \right)^{\frac{1}{2}}, \quad (11)$$

$$\mathbb{E} \left\| \mathbf{A} (\mathbf{I} - \mathbf{X}^\dagger \mathbf{X}) \right\| \leq \left(1 + \sqrt{\frac{k}{l-k-1}} \right) \sigma_{k+1}(\mathbf{A}) + \frac{e\sqrt{l}}{l-k} \left(\sum_{j \geq k+1} \sigma_j(\mathbf{A})^2 \right)^{\frac{1}{2}}. \quad (12)$$

Meanwhile, for arbitrary constants $u, t \geq 1$,

$$\left\| \mathbf{A} (\mathbf{I} - \mathbf{X}^\dagger \mathbf{X}) \right\|_F \leq \left(1 + t \sqrt{\frac{3k}{l-k+1}} \right) \left(\sum_{j \geq k+1} \sigma_j(\mathbf{A})^2 \right)^{\frac{1}{2}} + \frac{ute\sqrt{l}}{l-k+1} \sigma_{k+1}(\mathbf{A}) \quad (13)$$

with probability at least $1 - (2t^{-(l-k)} + e^{-u^2/2})$, and

$$\begin{aligned} \left\| \mathbf{A} (\mathbf{I} - \mathbf{X}^\dagger \mathbf{X}) \right\| &\leq \left[\left(1 + t \sqrt{\frac{3k}{l-k-1}} \right) \sigma_{k+1}(\mathbf{A}) + \frac{te\sqrt{l}}{l-k+1} \left(\sum_{j \geq k+1} \sigma_j(\mathbf{A})^2 \right)^{\frac{1}{2}} \right] \\ &\quad + \frac{ute\sqrt{l}}{l-k+1} \sigma_{k+1}(\mathbf{A}), \end{aligned} \quad (14)$$

with probability at least $1 - (2t^{-(l-k)} + e^{-u^2/2})$. In specific, with $t = l-k$ and $u = \sqrt{2(l-k)\log(l-k)}$, we have,

$$\left\| \mathbf{A} (\mathbf{I} - \mathbf{X}^\dagger \mathbf{X}) \right\|_F \leq \left(1 + \sqrt{3k(l-k)} \right) \left(\sum_{j \geq k+1} \sigma_j(\mathbf{A})^2 \right)^{\frac{1}{2}} + 4\sqrt{l(l-k)\log(l-k)} \sigma_{k+1}(\mathbf{A}), \quad (15)$$

$$\left\| \mathbf{A} (\mathbf{I} - \mathbf{X}^\dagger \mathbf{X}) \right\| \leq \left(1 + 6\sqrt{l(l-k)\log(l-k)} \right) \sigma_{k+1}(\mathbf{A}) + 3\sqrt{l} \left(\sum_{j \geq k+1} \sigma_j(\mathbf{A})^2 \right)^{\frac{1}{2}}, \quad (16)$$

with probability at least $1 - 3(l-k)^{-(l-k)}$.

In practice, [12], [31] suggest that a small constant oversampling, $\tilde{l} - k = 5$ or 10 , is sufficient to achieve a good approximation to \mathbf{A}_k . For a (nearly) full-rank matrix \mathbf{A} (i.e., $r \approx \min(m, n)$) that admits a good low-rank approximation $\mathbf{A}_k \approx \mathbf{A}$ for some $k \ll r$, a slight constant oversampling leads to an embedding dimension $\tilde{l} = k + O(1) \ll r$ such that, with high probability, $\tilde{l} = l$, and the sketch $\mathbf{X} \in \mathbb{R}^{l \times n}$ is full-rank.

Power iteration Both the theoretical error bounds in Lemma 2.1 and the empirical performance [12], [31] indicate that the rank- l approximation error $\|\mathbf{A}(\mathbf{I} - \mathbf{X}^\dagger \mathbf{X})\|_\xi$ depends on the spectrum decay of \mathbf{A} . In particular, $\widehat{\mathbf{A}}_l$ may suffer from a large error when the spectrum decay is slow. As a remedy, the power iteration and Krylov subspace methods are classical techniques for enhancing the spectrum decay of matrices.

Plain q power iterations

```

 $\mathbf{Z} \leftarrow \mathbf{S}\mathbf{A}$ 
for  $q = 1, \dots, q$  do
  if  $q$  is odd then
     $\mathbf{Z} \leftarrow \mathbf{Z}\mathbf{A}^T$ 
  else
     $\mathbf{Z} \leftarrow \mathbf{Z}\mathbf{A}$ 

```

Orthonormalized q power iterations

```

 $\mathbf{Z} \leftarrow \mathbf{S}\mathbf{A}$ 
for  $q = 1, \dots, q$  do
  if  $q$  is odd then
     $Z \leftarrow \text{ortho}(\mathbf{Z})\mathbf{A}^T$ 
  else
     $Z \leftarrow \text{ortho}(\mathbf{Z})\mathbf{A}$ 

```

In general, a sketch with q power iterations consist of $q + 1$ matrix-matrix multiplications with \mathbf{A} , and can be formed with $O(nnz(\mathbf{A})lq)$ operations. Starting with a column sketch, the power iterations result in a column sketch when q is even, and a row sketch when q is odd. Meanwhile, orthogonalizations (via unpivoted QR decomposition) are usually applied after each power iteration to maintain the numerical stability of the algorithm.

3 Column Selection

In this section, we discuss some common pivoting schemes for the second stage of the randomized skeleton selection. We start with the subproblem of the CSSP or ID. That is, we aim to select the skeleton columns greedily with pivoting on the sketch $\mathbf{X} = \mathbf{S}\mathbf{A}$ or the low-rank approximation $\widehat{\mathbf{A}}_l$ constructed in the first stage.

3.1 Low-rank Interpolative Decomposition (ID)

Given \mathbf{A} and k , the rank- k column-wise and row-wise interpolative decompositions (ID) of \mathbf{A} is defined as [5],

$$\mathbf{A}_{m \times n} \approx \mathbf{C}_{m \times k} \mathbf{V}_{k \times n}^T, \quad \mathbf{A}_{m \times n} \approx \mathbf{W}_{m \times k} \mathbf{R}_{k \times n}, \quad (17)$$

respectively, where $\mathbf{C} = \mathbf{A}(:, J_k)$ and $\mathbf{R} = \mathbf{A}(I_k, :)$ are subsets of columns and rows of \mathbf{A} specified by the k skeleton indices $J_k \subset [n]$, $I_k \subset [m]$, $|J_k| = |I_k| = k$. Intuitively, the ID aims to identify rank- k skeleton sets among the columns or rows of \mathbf{A} that maximize the respective spanning volumes. After the selection of the column or row skeletons, the IDs are constructed by solving the least square problems,

$$\mathbf{V}^T = \mathbf{C}^\dagger \mathbf{A} = \underset{\mathbf{V}' \in \mathbb{R}^{n \times k}}{\text{argmin}} : \|\mathbf{A} - \mathbf{C}\mathbf{V}'^T\|_F, \quad \mathbf{W} = \mathbf{A}\mathbf{R}^\dagger = \underset{\mathbf{W}' \in \mathbb{R}^{m \times k}}{\text{argmin}} : \|\mathbf{A} - \mathbf{W}'\mathbf{R}\|_F. \quad (18)$$

[2], [5] demonstrates the existence of a rank- k column skeleton set that satisfies,

$$\|\mathbf{A} - \mathbf{C}\mathbf{C}^\dagger \mathbf{A}\| = \|\mathbf{A} - \mathbf{C}\mathbf{V}^T\| \leq \sqrt{1 + k(n - k)} \|\mathbf{A} - \mathbf{A}_k\|. \quad (19)$$

However, identifying such an optimal skeleton set typically requires checking all the possible size- k subsets of the columns in \mathbf{A} , and is known to be NP-hard [10]. Alternatively, there exist polynomial time deterministic algorithms, such as the strong rank-revealing QR decomposition [4], for approximating the optimal skeleton set, and achieving similar multiplicative error bounds that are only looser than (19) by a constant factor.

3.2 Column Pivoted QR (CPQR)

The column pivoted QR decomposition (CPQR) is a common pivoting scheme in linear algebra that searches the entire active submatrix for the column with the maximal l_2 -norm at each step. The reduced column pivoted QR of \mathbf{A} takes the form $\mathbf{A}\Pi = \mathbf{Q}\mathbf{T}$, where $\Pi \in \mathbb{R}^{n \times n}$ is a column permutation of \mathbf{A} , $\mathbf{Q} \in \mathbb{R}^{m \times r}$ consists of an orthonormal base for the column space of \mathbf{A} , and $\mathbf{T} \in \mathbb{R}^{r \times n}$ is upper triangular. In particular, the column pivoting guarantees that $T_{ii} \geq \|\mathbf{T}(i : r, j)\|$ for all $1 \leq i \leq r$, $i < j \leq n$.

The CPQR enjoys certain rank-revealing guarantees. In particular, given $k < r$, the full rank CPQR can be truncated to rank- k by taking the first k pivoted columns,

$$\mathbf{A}\Pi = \mathbf{A} \begin{bmatrix} \Pi_1 & \Pi_2 \\ n \times k & n \times (n-k) \end{bmatrix} = \mathbf{Q}\mathbf{T} = \begin{bmatrix} \mathbf{Q}_1 & \mathbf{Q}_2 \\ m \times k & m \times (r-k) \end{bmatrix} \begin{bmatrix} \mathbf{T}_{11} & \mathbf{T}_{12} \\ k \times k & k \times (n-k) \\ \mathbf{0} & \mathbf{T}_{22} \\ (r-k) \times k & (r-k) \times (n-k) \end{bmatrix} \approx \mathbf{Q}_1 \begin{bmatrix} \mathbf{T}_{11} & \mathbf{T}_{12} \end{bmatrix}, \quad (20)$$

where \mathbf{Q} is orthogonal, and \mathbf{T}_{11} is an invertible upper triangular matrix. [4] demonstrates that the rank- k truncated CPQR is guaranteed to achieve the following,

$$\sigma_i(\mathbf{T}_{11}) \geq \frac{\sigma_i(\mathbf{A})}{\sqrt{r-i} \cdot 2^i}, \quad \sigma_j(\mathbf{T}_{22}) \leq \sigma_{k+j}(\mathbf{A}) \sqrt{r-k} \cdot 2^k, \quad \left| \left(\mathbf{T}_{11}^{-1} \mathbf{T}_{12} \right)_{ij} \right| \leq 2^{k-i}. \quad (21)$$

Moreover, [4] suggests that the CPQR usually provides a strong rank-revealing QR decomposition (strong RRQR) on general matrices. To be specific, a strong RRQR satisfies that for all $1 \leq i \leq k$ and $1 \leq j \leq r-k$, there exist low-degree polynomials $q_1(k, r)$ and $q_2(k, r)$ (in contrast to the exponential correlations in (21)) such that,

$$\sigma_i(\mathbf{T}_{11}) \geq \frac{\sigma_i(\mathbf{A})}{q_1(k, r)}, \quad \sigma_j(\mathbf{T}_{22}) \leq \sigma_{k+j}(\mathbf{A}) q_1(k, r), \quad \left| \left(\mathbf{T}_{11}^{-1} \mathbf{T}_{12} \right)_{ij} \right| \leq q_2(k, r). \quad (22)$$

However, there exist pathological matrices where the CPQR fails to be strongly rank-revealing.

Thanks to its rank-revealing property, the CPQR provides a greedy selection of skeleton columns for the ID or the CSSP [27]. In the realm of model reduction, this is also proposed as the Q-DEIM algorithm [22]. To be specific, we take the first k pivots of the CPQR as the column skeletons, and form the rank- k ID based on (20),

$$\mathbf{A}\Pi \approx \mathbf{Q}_1 \begin{bmatrix} \mathbf{T}_{11} & \mathbf{T}_{12} \end{bmatrix} = \mathbf{Q}_1 \mathbf{T}_{11} \begin{bmatrix} \mathbf{I} & \mathbf{T}_{11}^{-1} \mathbf{T}_{12} \end{bmatrix} = \mathbf{C} \mathbf{V}^T \Pi, \quad (23)$$

where $\mathbf{A} = \mathbf{C} \mathbf{V}^T$, $\mathbf{C} = \mathbf{Q}_1 \mathbf{T}_{11} = \mathbf{A}\Pi(:, 1 : k)$, and $\mathbf{V}^T = \begin{bmatrix} \mathbf{I} & \mathbf{T}_{11}^{-1} \mathbf{T}_{12} \end{bmatrix} \Pi^T = \mathbf{T}_{11}^{-1} \mathbf{Q}_1^T \mathbf{A} = \mathbf{C}^\dagger \mathbf{A}$. With the worst-case rank-revealing guarantees for the CPQR (21), the rank- k column-wise ID (23) satisfies that,

$$\|\mathbf{A} - \mathbf{C} \mathbf{V}^T\| = \left\| \mathbf{A} - \mathbf{Q}_1 \begin{bmatrix} \mathbf{T}_{11} & \mathbf{T}_{12} \end{bmatrix} \right\| = \|\mathbf{T}_{22}\| \leq \sqrt{r-k} 2^k \|\mathbf{A} - \mathbf{A}_k\|. \quad (24)$$

In spite of the weaker rank-revealing guarantee (21) in certain contrived cases, empirically, the CPQR is usually a more efficient alternative to the strong rank-revealing QR for the greedy skeleton selection with pivoting.

Randomized column selection via CPQR The skeleton selection with the CPQR can be easily coupled with sketching [27], as demonstrated in Algorithm 1, which comes with two benefits. First, embedding the high dimensional column space to a lower dimension $\tilde{l} \ll m$ improves the efficiency. That is, applying the CPQR on a sketch of \mathbf{A} , instead of \mathbf{A} , reduces

the complexity of the pivoting step from $O(lmn)$ to $O(l^2n)$. Second, the randomization in the sketching step makes the algorithm less vulnerable to the adversarial inputs. Moreover, the column sketch \mathbf{X} in Algorithm 1 can be coupled with power iterations. In practice, constructing the column sketch with one power iteration without orthonormalization brings observable improvement in the approximation accuracy for matrices with slow spectrum decay.

Algorithm 1 Randomized CPQR skeleton selection

Input: $\mathbf{A} \in \mathbb{R}^{m \times n}$, target rank $k < r = \text{rank}(\mathbf{A})$, sample size $\tilde{l} = k + O(1)$

Output: A set of skeleton column indices $J \subset [n]$ such that $|J| = l$ and $\mathbf{C} = \mathbf{A}(:, J)$

1: Draw an oblivious l_2 -subspace embedding $\mathbf{\Gamma} \in \mathbb{R}^{\tilde{l} \times m}$

2: Construct the sketch of the column space with $O(1)$ oversampling $\mathbf{X} = \mathbf{\Gamma} \mathbf{A} \in \mathbb{R}^{\tilde{l} \times n}$

3: Perform the CPQR on \mathbf{X} ,

$$\mathbf{X}(:, J_n) = \mathbf{X} \mathbf{\Pi} = \mathbf{Q}_1 \begin{bmatrix} \mathbf{T}_1 & \mathbf{T}_2 \\ \tilde{l} \times l & l \times (n-l) \end{bmatrix},$$

4: $J = J_n(1 : l)$, $\mathbf{C} = \mathbf{A}(:, J)$

The rank- l approximation error of the column ID constructed by the randomized CPQR lies within a constant factor of $\|\mathbf{A} - \mathbf{A}\mathbf{X}^\dagger\mathbf{X}\|_\xi$. In particular, we denote the column pivoted QR decomposition of \mathbf{X} as following,

$$\mathbf{X} \begin{smallmatrix} \mathbf{\Pi} \\ \tilde{l} \times n \end{smallmatrix} = \mathbf{X} \begin{bmatrix} \mathbf{\Pi}_c & \mathbf{\Pi}_{c^c} \\ n \times l & n \times (n-l) \end{bmatrix} = \mathbf{Q} \begin{smallmatrix} \mathbf{T} \\ \tilde{l} \times l \end{smallmatrix} = \mathbf{Q} \begin{bmatrix} \mathbf{T}_1 & \mathbf{T}_2 \\ l \times l & l \times (n-l) \end{bmatrix},$$

where $\mathbf{\Pi}_c$ is a submatrix of the column permutation corresponding to the l column skeletons selected for the ID. \mathbf{Q} is an orthogonal matrix. \mathbf{T}_1 is invertible and upper triangular. The column pivoting guarantees that $T_{ii} \geq \|\mathbf{T}(i : l, j)\|$ for all $1 \leq i < j \leq l$. Since \mathbf{T}_1 is invertible, we can define a rank- l oblique projector onto the row space of \mathbf{X} such that,

$$\mathcal{P}_X := \mathbf{\Pi}_c (\mathbf{X} \mathbf{\Pi}_c)^\dagger \mathbf{X} = \mathbf{\Pi}_c \mathbf{T}_1^{-1} \mathbf{Q}^T \mathbf{X},$$

such that $\mathbf{X} \mathcal{P}_X = \mathbf{Q} \mathbf{Q}^T \mathbf{X} = \mathbf{X}$.

Theorem 3.1. *For an embedding dimension \tilde{l} such that $k+4 \leq \tilde{l} \leq \text{rank}(\mathbf{A})$, let l be the rank of the column sketch $\mathbf{X} \in \mathbb{R}^{\tilde{l} \times n}$. Then, the rank- l column ID constructed with skeletons \mathbf{C} selected by Algorithm 1, and $\mathbf{V} = \mathbf{C}^\dagger \mathbf{A}$ satisfies that,*

$$\|\mathbf{A} - \mathbf{C}\mathbf{V}^T\|_\xi \leq \eta^{qr} \cdot \|\mathbf{A}(\mathbf{I} - \mathbf{X}^\dagger \mathbf{X})\|_\xi, \quad (25)$$

where $\eta^{qr} := \|\mathbf{I} - \mathcal{P}_X\|$ has a dimension-dependent upper bound, $\xi = 2, F$, and $\|\mathbf{A}(\mathbf{I} - \mathbf{X}^\dagger \mathbf{X})\|_\xi$ satisfies the set of expectation and tail bounds in Lemma 2.1.

Proof. We first observe that, since $\mathbf{X}(\mathbf{I} - \mathcal{P}_X) = \mathbf{0}$,

$$\|\mathbf{A}(\mathbf{I} - \mathcal{P}_X)\|_\xi = \|\mathbf{A}(\mathbf{I} - \mathbf{X}^\dagger \mathbf{X})(\mathbf{I} - \mathcal{P}_X)\|_\xi \leq \|(\mathbf{I} - \mathcal{P}_X)\| \|\mathbf{A}(\mathbf{I} - \mathbf{X}^\dagger \mathbf{X})\|_\xi. \quad (26)$$

Meanwhile, since $\mathbf{\Gamma} \mathbf{A} \mathbf{\Pi}_c = \mathbf{\Gamma} \mathbf{C}$ is full-rank, $\mathbf{C} = \mathbf{A} \mathbf{\Pi}_c$ must have full column rank, and therefore $\mathbf{C}^\dagger = (\mathbf{C}^T \mathbf{C})^{-1} \mathbf{C}^T$, and the corresponding ID of \mathbf{A} with column skeletons \mathbf{C} can be expressed as

$$\mathbf{C} \mathbf{C}^\dagger \mathbf{A} = \mathbf{A} \mathbf{\Pi}_c (\mathbf{C}^T \mathbf{C})^{-1} \mathbf{C}^T \mathbf{A} = \mathbf{A} \mathcal{P}_C,$$

where $\mathcal{P}_C := \mathbf{\Pi}_c \left(\mathbf{C}^T \mathbf{C} \right)^{-1} \mathbf{C}^T \mathbf{A}$ is a rank- l oblique projector such that

$$\mathcal{P}_C \mathcal{P}_X = \mathbf{\Pi}_c \left(\mathbf{C}^T \mathbf{C} \right)^{-1} \mathbf{C}^T \mathbf{A} \mathbf{\Pi}_c \left(\mathbf{X} \mathbf{\Pi}_c \right)^{-1} \mathbf{X} = \mathcal{P}_X.$$

Then we can find the upper bound for the error of the rank- l column ID,

$$\begin{aligned} \left\| (\mathbf{I} - \mathbf{C} \mathbf{C}^\dagger) \mathbf{A} \right\|_\xi &= \left\| \mathbf{A} (\mathbf{I} - \mathcal{P}_C) \right\|_\xi = \left\| \mathbf{A} (\mathbf{I} - \mathcal{P}_C) (\mathbf{I} - \mathcal{P}_X) \right\|_\xi \\ &= \left\| (\mathbf{I} - \mathbf{C} \mathbf{C}^\dagger) \mathbf{A} (\mathbf{I} - \mathcal{P}_X) \right\|_\xi \\ &\leq \left\| \mathbf{I} - \mathbf{C} \mathbf{C}^\dagger \right\| \left\| \mathbf{A} (\mathbf{I} - \mathcal{P}_X) \right\|_\xi. \end{aligned}$$

Since $\left\| \mathbf{I} - \mathbf{C} \mathbf{C}^\dagger \right\| = 1$, combining the inequality (26), we have

$$\left\| \mathbf{A} - \mathbf{C} \mathbf{V}^T \right\|_\xi = \left\| (\mathbf{I} - \mathcal{P}_X) \right\| \left\| \mathbf{A} (\mathbf{I} - \mathbf{X}^\dagger \mathbf{X}) \right\|_\xi = \eta^{qr} \cdot \left\| \mathbf{A} (\mathbf{I} - \mathbf{X}^\dagger \mathbf{X}) \right\|_\xi.$$

□

Lemma 3.2. *In the same setting as Theorem 3.1,*

$$\eta^{qr} = \left\| \mathbf{I} - \mathcal{P}_X \right\| \leq \sqrt{1 + (n - l) \cdot 4^{l-1}}. \quad (27)$$

Proof. We observe that η^{qr} can be expanded as following,

$$\left\| \mathbf{I} - \mathcal{P}_X \right\|_\xi = \left\| \mathbf{I} - \mathbf{\Pi}_c \mathbf{T}_1^{-1} \mathbf{Q} \mathbf{X} \right\|_\xi = \left\| \mathbf{\Pi}_{c^c} - \mathbf{\Pi}_c \mathbf{T}_1^{-1} \mathbf{T}_2 \right\|_\xi = \left\| \begin{bmatrix} \mathbf{T}_1^{-1} & \mathbf{T}_2 \\ l \times l & l \times (n-l) \\ & -\mathbf{I} \\ (n-l) \times (n-l) & \end{bmatrix} \right\|_\xi.$$

Leveraging the rank-revealing guarantees of the column pivoted QR in (21),

$$\left| \left(\mathbf{T}_1^{-1} \mathbf{T}_2 \right)_{ij} \right| \leq 2^{l-i},$$

which can be shown via backward substitution and induction. Therefore,

$$\left\| \mathbf{I} - \mathcal{P}_X \right\|_\xi \leq \sqrt{1 + \left\| \mathbf{T}_1^{-1} \mathbf{T}_2 \right\|^2} \leq \sqrt{1 + (n - l) \cdot 4^{l-1}}.$$

□

3.3 LU with Partial Pivoting (LUPP)

The Gaussian elimination with partial pivoting (LUPP) is a common pivoting scheme for the LU matrix decomposition that searches the leading column of the active submatrix for the pivot with the maximal absolute value. To be specific, the row-wise LUPP finds a row permutation $I \in [m]^m$ corresponding to $\mathbf{\Pi} = \mathbf{I}(:, I)$, a lower triangular matrix $\mathbf{L} \in \mathbb{R}^{m \times r}$, and an upper triangular matrix $\mathbf{T} \in \mathbb{R}^{r \times n}$ such that $\mathbf{A}(I, :) = \mathbf{\Pi}^T \mathbf{Y} = \mathbf{L} \mathbf{T}$. The first r pivoted rows in I are linearly independent, and form a base for the row space of \mathbf{A} . Furthermore, the row pivoting guarantees that $L_{jj} = 1$ and $|L_{ij}| \leq 1$ for all $1 \leq j \leq n$, $j < i \leq m$. In practice, the LUPP can be computed more efficiently than the CPQR with high performance benchmarks such as the LAPACK [16].

However, since the partial pivoting only search the active subset of the leading column for each pivot, without viewing the entire active submatrix, the LUPP is vulnerable to the rank-deficient systems, and fails to enjoy similar spectrum-revealing properties as the column pivoted QR (21), especially on the sparse matrices. There exist more sophisticated LU-based pivoting schemes, such as the spectrum revealing LU decomposition [24], that achieves similar spectral bounds as the strong rank-revealing QR (22). But the empirical efficiency of these pivoting schemes is hardly comparable to the LU with partial pivoting. Nevertheless, the LUPP is numerically stable, and is known to perform well on general full-rank matrices [3]. To leverage the efficiency of the LUPP while avoiding its vulnerabilities, instead of applying the LUPP directly on \mathbf{A} with potential rank-deficiency, to select the column skeletons for \mathbf{A} , we can apply the LUPP on a proper full-rank representation of the row space.

Discrete empirical interpolation method (DEIM) The discrete empirical interpolation method (DEIM) [22], [23] is a deterministic greedy skeleton selection algorithm originated from the realm of model reduction. To select the column skeletons of rank k exactly, the DEIM takes the first k right singular vectors of \mathbf{A} , $\mathbf{W} = [\mathbf{w}_1, \dots, \mathbf{w}_k] \in \mathbb{R}^{n \times k}$, as the input, and selects a set of k columns indexed by $J \subset [n]$, as shown in Algorithm 2.

Algorithm 2 DEIM point selection

Input: $\mathbf{W} \in \mathbb{R}^{n \times k}$ with orthonormal columns, $n \geq k$
Output: The skeleton indices $J \subset [n]$ such that $|J| = k$

- 1: $\mathbf{w} = \mathbf{W}(:, 1)$
- 2: $[\sim, p_1] = \max(|\mathbf{w}|)$
- 3: $J = [p_1]$
- 4: **for** $j = 2 : k$ **do**
- 5: $\mathbf{w} = \mathbf{W}(:, j)$
- 6: $\mathbf{c} = \mathbf{W}(J, 1 : j - 1)^{-1} \mathbf{w}(J)$
- 7: $\mathbf{r} = \mathbf{w} - \mathbf{W}(:, 1 : j - 1) \mathbf{c}$
- 8: $[\sim, p_j] = \max(|\mathbf{r}|)$
- 9: $J = [J; p_j]$

The greedy point selection with DEIM in Algorithm 2 is equivalent to the LU with row pivoting, in the sense that they provide the same ordering of rows, as illustrated in Appendix A. Thanks to the leading singular vectors, the skeleton selection with DEIM leverages the empirical efficiency of the LUPP, while circumvents its disadvantages. Specifically, the leading singular vectors \mathbf{V} is guaranteed to be full column rank, and comes with a prior ordering in columns. Therefore, the DEIM skeleton selection usually provides a nearly optimal set of skeletons [23].

[23] demonstrates that the rank- k column ID constructed with the skeletons \mathbf{C} selected by the DEIM point selection (Algorithm 2) and $\mathbf{V}^T = \mathbf{C}^\dagger \mathbf{A}$ satisfies that

$$\|\mathbf{A} - \mathbf{C}\mathbf{V}^T\|_2 \leq \eta \cdot \sigma_{k+1}(\mathbf{A}),$$

where η depends only on the leading k right singular vectors $\mathbf{W} \in \mathbb{R}^{n \times k}$ of \mathbf{A} such that $\eta < \sqrt{\frac{nk}{3}} 2^k$. In addition, [23] shows that this upper bound for η is asymptotically tight by instantiating a \mathbf{W} where η grows exponentially. Nevertheless, such pathological matrices almost never occur in practice.

The deterministic DEIM skeleton selection requires the singular vectors of \mathbf{A} as the input. For a large-scale matrix \mathbf{A} , the exact evaluation of the SVD is prohibitively expensive. Nevertheless, leveraging the low-rank approximation constructed with sketching, the leading k singular vectors of \mathbf{A} can be approximated efficiently with the randomized SVD algorithm [12], as shown

in Algorithm 3. It is worth to notice that, in Algorithm 3, $\mathbf{B} \in \mathbb{R}^{l \times n}$ is equivalent to a column sketch with one orthonormalized power iteration. Meanwhile, with \mathbf{Q} and $\widehat{\mathbf{U}}$, the left singular vectors can be approximated efficiently with matrix multiplication $\mathbf{U} = \mathbf{Q}\widehat{\mathbf{U}}$ in $O(ml^2)$ operations, and the row skeletons can be selected accordingly.

Algorithm 3 Randomized DEIM skeleton selection

Input: $\mathbf{A} \in \mathbb{R}^{m \times n}$, target rank $k < r = \text{rank}(\mathbf{A})$, sample size $\tilde{l} = k + O(1)$

Output: A set of skeleton column indices $J \subset [n]$ such that $|J| = l$ and $\mathbf{C} = \mathbf{A}(:, J)$

- 1: Draw an oblivious l_2 -subspace embedding $\mathbf{\Omega} \in \mathbb{R}^{\tilde{l} \times n}$
- 2: Construct the sketch of the column space with $O(1)$ oversampling $\mathbf{Y} = \mathbf{A}\mathbf{\Omega} \in \mathbb{R}^{m \times \tilde{l}}$
- 3: $\mathbf{Q} = \text{ortho}(\mathbf{Y}) \in \mathbb{R}^{m \times l}$
- 4: $\mathbf{B} = \mathbf{Q}^T \mathbf{A}$
- 5: Compute SVD of \mathbf{B} :

$$\mathbf{B} = \widehat{\mathbf{U}} \begin{matrix} \Sigma \\ l \times l \end{matrix} \mathbf{V}^T \begin{matrix} \\ l \times n \end{matrix}$$

- 6: Select the l column skeletons, indexed by J , by applying Algorithm 2 on \mathbf{V}
- 7: $\mathbf{C} = \mathbf{A}(:, J)$

Randomized column selection via LUPP As a simpler randomized alternative to the DEIM that avoids the evaluation or approximation of the SVD, with an appropriate subspace embedding, the leading pivots of the LU with column pivoting on the sketch $\mathbf{X} = \mathbf{S}\mathbf{A}$ provide good approximations to the optimal column skeletons. With dimension reduction, the LUPP can be applied to the sketch \mathbf{X} efficiently. But more essentially, the randomization with subspace embedding is necessary for the skeleton selection with the LUPP because it provides a random full-rank sketch with high probability where the LUPP achieves reasonable performance. Since the LUPP tends to be less stable on sparse matrices, when the input matrix \mathbf{A} is sparse, we recommend using the dense subspace embeddings (i.e., \mathbf{S} that yields a dense sketch \mathbf{X}) such as the Gaussian random matrix or the SRFT. The power iterations can also be coupled with the column sketch \mathbf{X} in Algorithm 4. As for the randomized CPQR, one plain power iteration is sufficient to achieve observable improvement in the approximation accuracy for matrices with slow spectrum decay, without considerably sacrificing the efficiency.

Algorithm 4 Randomized LUPP skeleton selection

Input: $\mathbf{A} \in \mathbb{R}^{m \times n}$, target rank $k < r = \text{rank}(\mathbf{A})$, sample size $\tilde{l} = k + O(1)$

Output: A set of skeleton column indices $J \subset [n]$ such that $|J| = l$ and $\mathbf{C} = \mathbf{A}(:, J)$

- 1: Draw an oblivious l_2 -subspace embedding $\mathbf{\Gamma} \in \mathbb{R}^{\tilde{l} \times m}$
- 2: Construct the sketch of the column space with $O(1)$ oversampling $\mathbf{X} = \mathbf{\Gamma}\mathbf{A} \in \mathbb{R}^{\tilde{l} \times n}$
- 3: Perform the LUPP on \mathbf{X}^T ,

$$\mathbf{X}(:, J_n)^T = \mathbf{\Pi}^T \mathbf{X}^T = \begin{bmatrix} \mathbf{L}_1 \\ l \times l \\ \mathbf{L}_2 \\ (n-l) \times l \end{bmatrix}_{l \times \tilde{l}} \mathbf{T}_{\tilde{l}}$$

If a zero pivot is encountered (i.e., $\tilde{l} > l$), restart the algorithm

- 4: $J = J_n(1 : l)$, $\mathbf{C} = \mathbf{A}(:, J)$

The similar analysis as that for the randomized CPQR indicates that the rank- l approximation error of the column ID constructed via the randomized LUPP is also bounded by a constant

factor of $\|\mathbf{A} - \mathbf{A}\mathbf{X}^\dagger \mathbf{X}\|_\xi$. Upon a transpose, we can express the LU with row pivoting of \mathbf{X}^T as

$$\mathbf{X}_{l \times n} \mathbf{\Pi}_{n \times n} = \mathbf{X} \begin{bmatrix} \mathbf{\Pi}_c & \mathbf{\Pi}_{c^c} \\ n \times l & n \times (n-l) \end{bmatrix} = \mathbf{T}^T \mathbf{L}^T = \mathbf{T}_{l \times l}^T \begin{bmatrix} \mathbf{L}_1^T & \mathbf{L}_2^T \\ l \times l & l \times (n-l) \end{bmatrix},$$

where $\mathbf{\Pi}_c$ is a submatrix of the column permutation corresponding to the l column skeletons selected for the ID. $\mathbf{L}_1, \mathbf{T} \in \mathbb{R}^{l \times l}$ are invertible lower and upper triangular matrices, respectively. In particular, with the row pivoting, $L_{ii} = 1$ for all $i = 1, \dots, l$, and $|L_{ij}| \leq 1$ for all $1 \leq j \leq l$, $j+1 \leq i \leq n$. Since $\mathbf{X}\mathbf{\Pi}_c = (\mathbf{L}_1\mathbf{T})^T \in \mathbb{R}^{l \times l}$ is invertible, we can define a rank- l oblique projector onto the range of \mathbf{Y} such that,

$$\mathcal{P}_X := \mathbf{\Pi}_c (\mathbf{X}\mathbf{\Pi}_c)^{-1} \mathbf{X}$$

such that $\mathbf{X}\mathcal{P}_X = \mathbf{X}$.

Corollary 3.2.1. *For an embedding dimension \tilde{l} such that $k+4 \leq \tilde{l} \leq \text{rank}(\mathbf{A})$, let l be the rank of the column sketch $\mathbf{X} \in \mathbb{R}^{\tilde{l} \times n}$. Then, the rank- l column ID constructed with skeletons \mathbf{C} selected by Algorithm 4, and $\mathbf{V} = \mathbf{C}^\dagger \mathbf{A}$ satisfies that,*

$$\|\mathbf{A} - \mathbf{C}\mathbf{V}^T\|_\xi \leq \eta^{lu} \cdot \|\mathbf{A}(\mathbf{I} - \mathbf{X}^\dagger \mathbf{X})\|_\xi, \quad (28)$$

where $\eta^{lu} := \|\mathbf{I} - \mathcal{P}_X\|$ is bounded up by a constant depending only on n, l , $\xi = 2, F$, and $\|\mathbf{A}(\mathbf{I} - \mathbf{X}^\dagger \mathbf{X})\|_\xi$ satisfies the set of expectation and tail bounds in Lemma 2.1.

Lemma 3.3. *In the same setting as Corollary 3.2.1,*

$$\eta^{lu} = \|\mathbf{I} - \mathcal{P}_X\| \leq \sqrt{1 + (n-l) \cdot 4^{l-1}} \quad (29)$$

Proof. We first observe that

$$\|\mathbf{I} - \mathcal{P}_X\|_\xi = \left\| \mathbf{I} - \mathbf{\Pi}_c (\mathbf{X}\mathbf{\Pi}_c)^{-1} \mathbf{X} \right\|_\xi = \left\| \mathbf{\Pi}_{c^c} - \mathbf{\Pi}_c \mathbf{L}_1^{-T} \mathbf{L}_2^T \right\|_\xi = \left\| \begin{bmatrix} \mathbf{L}_1^{-T} & \mathbf{L}_2^T \\ l \times l & l \times (n-l) \\ -\mathbf{I} & \\ (n-l) \times (n-l) & \end{bmatrix} \right\|_\xi.$$

The matrices $\mathbf{L}_1 \in \mathbb{R}^{l \times l}$ and $\mathbf{L}_2 \in \mathbb{R}^{(n-l) \times l}$ contain the multipliers from the row pivoted LU, and therefore \mathbf{L} satisfies that $L_{ii} = 1$ for all $i = 1, \dots, l$, and $|L_{ij}| \leq 1$ for all $1 \leq j \leq l$, $j+1 \leq i \leq n$. In specific, we denote $\tilde{\mathbf{X}}^{(0)} = \mathbf{X}$. Let $\tilde{\mathbf{X}}^{(t)}$ be the resulted matrix after t steps of row pivoted Gaussian elimination. Let $\mathbf{\Pi}_{(t+1)}^T$ be the t -th row pivoting that is applied on $\tilde{\mathbf{X}}^{(t)}$, and $(\mathbf{X}^{(t)})^T = \mathbf{\Pi}_{(t+1)}^T (\tilde{\mathbf{X}}^{(t)})^T$ after the row pivoting. Then entry-wisely, $\mathbf{L} \in \mathbb{R}^{n \times l}$ can be expressed as,

$$L_{ij} = \begin{cases} \mu_{ij} & i > j \\ 1 & i = j \\ 0 & i < j \end{cases}, \quad \mu_{ij} = \frac{X_{ji}^{(j-1)}}{Y_{ii}^{(j-1)}} \in [-1, 1], \quad j = \underset{s=j, \dots, n}{\text{argmax}} : |Y_{js}^{(j-1)}|.$$

We can construct \mathbf{L}_1^{-1} by solving $\mathbf{L}_1 \mathbf{x} = \mathbf{e}_j$ for all canonical bases \mathbf{e}_j , $j = 1, \dots, l$, via the

forward substitution,

$$\begin{aligned}
x_i &= 0 \quad \forall i < j \\
x_j &= 1 \\
x_{j+1} &= -\mu_{j+1,j} \\
x_{j+2} &= \mu_{j+2,j+1}\mu_{j+1,j} - \mu_{j+2,j} \\
&\dots \\
x_i &= \sum_{P_{i \rightarrow j} \subset E} \left((-1)^{|P|} \prod_{(p,q) \in P_{i \rightarrow j}} \mu_{p,q} \right) \quad \forall i > j,
\end{aligned} \tag{30}$$

where in the case that $i > j$, we express x_i with a weighted fully connected directed graph $G = (V, E, \mu)$ such that $V = \{j, \dots, i\}$, $E = \{p \rightarrow q : p, q \in V, p > q\}$, and $\mu \in [-1, 1]^{(i-j)(i-j+1)/2}$ with weights $\mu_{p,q}$. We denote a path from i to j as $P_{i \rightarrow j} \subset E$, consisting of edges $(p, q) \in P_{i \rightarrow j}$. Overall, there are

$$\sum_{s=0}^{i-j-1} \binom{i-j-1}{s} = 2^{i-j-1}$$

possible paths from i to j , with products of weights bounded in $[-1, 1]$. Therefore,

$$\left| \left(\mathbf{L}_1^{-1} \right)_{ij} \right| = |x_i| \leq 2^{i-j-1}, \quad \forall 1 \leq j < i \leq l.$$

Then leveraging the fact that $\left| \left(\mathbf{L}_2 \right)_{ij} \right| \leq 1$ for all $1 \leq i \leq m-l$, $1 \leq j \leq l$, we have an entry-wise upper bound for $\mathbf{L}_2 \mathbf{L}_1^{-1}$,

$$\left| \left(\mathbf{L}_2 \mathbf{L}_1^{-1} \right)_{ij} \right| \leq 2^{l-j}, \quad \forall 1 \leq i \leq m-l, \quad 1 \leq j \leq l.$$

Consequentially,

$$\left\| \begin{bmatrix} -\mathbf{I} & \mathbf{L}_2 \mathbf{L}_1^{-1} \end{bmatrix} \right\| \leq \sqrt{1 + \left\| \mathbf{L}_2 \mathbf{L}_1^{-1} \right\|^2} \leq \sqrt{1 + (m-l) \cdot 4^{l-1}}.$$

□

We observe that, in spite of the exponential dependency on l in the worst scenario (27, 29), both η^{qr} and η^{lu} grow much slower with respect to l in practice. For instance, knowing that

$$\eta^{lu} \leq \sqrt{1 + \left\| \mathbf{L}_2 \mathbf{L}_1^{-1} \right\|},$$

Figure 1 shows the values of $\left\| \mathbf{L}_2 \mathbf{L}_1^{-1} \right\|_\xi$ ($\xi = 2, F$) for the sketches of some empirical data sets, as well as those for the standard Gaussian matrices with the same size. The average-case stability analysis for the Gaussian elimination on random matrices in [3] provides rationale for such empirical observation. In specific, when the Gaussian embedding is used, with a mild assumption $l \leq 1024$ (which is usually satisfied by the low-rank decompositions in practice), $\langle \eta^{lu} \rangle$ grows in a low-degree polynomial order with respect to l in the average cases,

$$\langle \eta^{lu} \rangle \lesssim l^{\frac{13}{6}} \sqrt{n-l}, \tag{31}$$

as discussed in Appendix B.

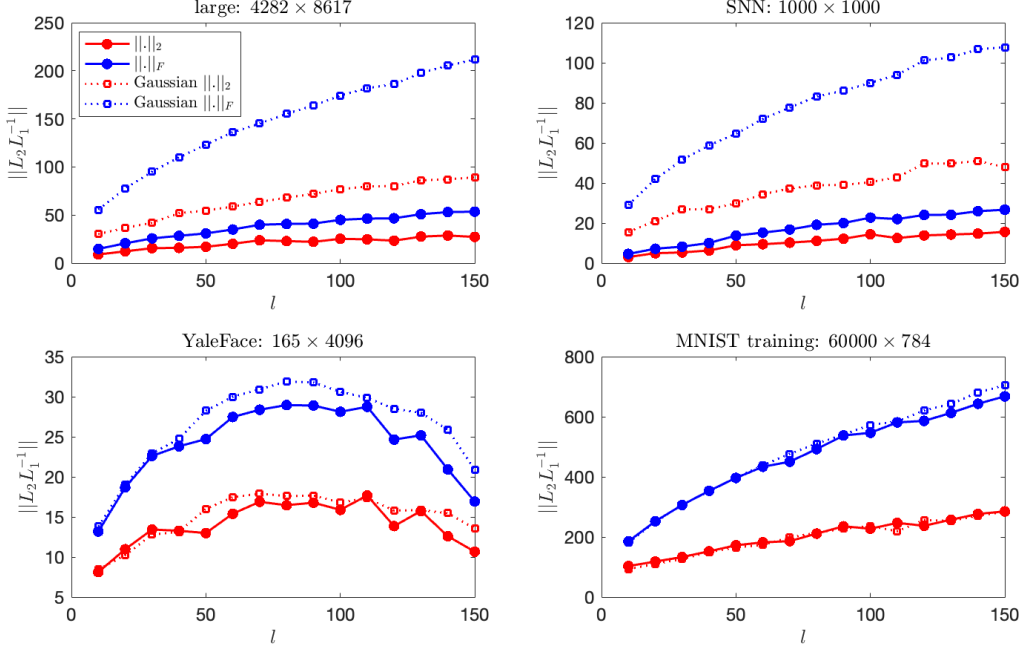


Figure 1: $\|\mathbf{L}_2 \mathbf{L}_1^{-1}\|_\xi$ for $\xi = 2, F$. The solid lines come from the average of 10 independent sample matrices with size $n \times l$ of various empirical data sets (with sizes $m \times n$ labeled in the title), while the dashes come from the average of 10 standard Gaussian random matrices with the same sizes $n \times l$ as the corresponding sketches.

Abbreviation	Algorithm	Stage 1	Stage 2
Rand-CPQR	Algorithm 1	$O(T_s(k, \mathbf{A}))$	$O(nk^2)$
Rand-CPQR-p1	one power iteration	$O(T_s(k, \mathbf{A}^T) + \text{nnz}(\mathbf{A})k)$	$O(nk^2)$
Rand-DEIM	Algorithm 3	$O(T_s(k, \mathbf{A}^T) + (m+n)k^2 + \text{nnz}(\mathbf{A})k)$	$O(nk^2)$
Rand-LUPP	Algorithm 4	$O(T_s(k, \mathbf{A}))$	$O(nk^2)$
Rand-LUPP-p1	one power iteration	$O(T_s(k, \mathbf{A}^T) + \text{nnz}(\mathbf{A})k)$	$O(nk^2)$

Table 2: The asymptotic complexities of the pivoting based randomized column skeleton selection algorithms.

4 CUR Decomposition

With algorithms for column selection, in this section, we consider the problem of selecting skeletons on both sides of \mathbf{A} . We first introduce two related forms of low-rank decompositions based on the row and column skeletons, namely the two-sided ID and the CUR decomposition. Then, we discuss several pivoting based procedures for the row selection, using either the low-rank decomposition constructed in the first stage of column selection, or the selected column skeletons.

4.1 Two-sided ID and CUR Decomposition

Two-sided ID Given the matrix \mathbf{A} and a target rank $k < \text{rank}(\mathbf{A})$, the rank- k two-sided interpolative decomposition (two-sided ID) of \mathbf{A} is given by

$$\underset{m \times n}{\mathbf{A}} \approx \underset{m \times k}{\mathbf{W}} \underset{k \times k}{\mathbf{A}_s} \underset{k \times n}{\mathbf{V}^T}, \quad (32)$$

where for the rank- k row and column skeletons indexing by $I_k \subset [m]$, $J_k \subset [n]$, $|I_k| = |J_k| = k$, $\mathbf{A}_s = \mathbf{A}(I_k, J_k)$ is invertible, and \mathbf{W}, \mathbf{V} are formed as (18), respectively. It is worth to point out that the skeleton submatrix \mathbf{A}_s tends to share the similar spectrum decay as \mathbf{A} , and therefore, for a matrix \mathbf{A} that admits low-rank approximations, the corresponding \mathbf{A}_s is usually ill-conditioned.

Low-rank CUR decomposition The two-sided ID (32) can be reformulated as a CUR decomposition (1) such that

$$\mathbf{A} \approx \mathbf{W} \mathbf{A}_s \mathbf{V}^T = \mathbf{C} \mathbf{U} \mathbf{R}, \quad (33)$$

where $\mathbf{C} = \mathbf{A}(:, J_k) \in \mathbb{R}^{m \times k}$, $\mathbf{R} = \mathbf{A}(I_k, :) \in \mathbb{R}^{k \times n}$, and

$$\mathbf{U} = \mathbf{C}^\dagger \mathbf{A} \mathbf{R}^\dagger = \underset{\mathbf{U}' \in \mathbb{R}^{k \times k}}{\text{argmin}} \|\mathbf{A} - \mathbf{C} \mathbf{U}' \mathbf{R}\|_F.$$

Proposition 4.1. *With the identical sets of row and column skeletons, $I_k \subset [m]$ and $J_k \subset [n]$, the two-sided ID and the CUR decomposition are equivalent in the exact arithmetic, but differ in numerical stability.*

To see the equivalence, we first observe that by the construction of the two-sided ID, $\mathbf{C} = \mathbf{W} \mathbf{A}_s$ and $\mathbf{R} = \mathbf{A}_s \mathbf{V}^T$. Since \mathbf{A}_s is invertible by construction, the two-sided ID can be reformulated as following,

$$\mathbf{W} \mathbf{A}_s \mathbf{V}^T = \mathbf{C} \mathbf{V}^T = \mathbf{W} \mathbf{R} = (\mathbf{W} \mathbf{A}_s) \mathbf{A}_s^{-1} (\mathbf{A}_s \mathbf{V}^T) = \mathbf{C} \mathbf{A}_s^{-1} \mathbf{R}. \quad (34)$$

Meanwhile, since $\mathbf{V}^T = \mathbf{C}^\dagger \mathbf{A} = \mathbf{A}_s^{-1} \mathbf{R}$, and $\mathbf{R} \mathbf{R}^\dagger = \mathbf{I} \in \mathbb{R}^{k \times k}$,

$$\mathbf{A}_s^{-1} = \mathbf{C}^\dagger \mathbf{A} \mathbf{R}^\dagger = \mathbf{U}. \quad (35)$$

Nevertheless, construction of the CUR decomposition is numerically less stable than that of the two-sided ID. Since the skeleton submatrix \mathbf{A}_s is usually ill-conditioned for a matrix \mathbf{A} that admits rapid spectrum decay, direct inversion of \mathbf{A}_s can be numerically catastrophic. A stable construction of \mathbf{U} involves solving two overdetermined least square problems with a backward stable solver.

4.2 Row Selection

We start with a rank- k column skeleton $\mathbf{C} \in \mathbb{R}^{m \times l}$ selected by one of the methods described in Section 3. Since \mathbf{C} has full column rank by construction, we can select the row skeletons by computing the exact row ID of \mathbf{C} via pivoting. In particular, with the CPQR on \mathbf{C}^T , we have

$$\mathbf{C}^T \begin{bmatrix} \mathbf{\Pi}_r & \mathbf{\Pi}_{r^c} \\ m \times l & m \times (m-l) \end{bmatrix} = \mathbf{Q} \begin{bmatrix} \mathbf{T}_1 & \mathbf{T}_2 \\ l \times l & l \times (m-l) \end{bmatrix} = \mathbf{A}_s^T \begin{bmatrix} \mathbf{I} & \mathbf{T}_1^{-1} \mathbf{T}_2 \\ l \times l & l \times (m-l) \end{bmatrix}. \quad (36)$$

Meanwhile, with the LU with row pivoting on \mathbf{C} , we have

$$\begin{bmatrix} \mathbf{\Pi}_r^T \\ l \times m \\ \mathbf{\Pi}_{rc}^T \\ (m-l) \times m \end{bmatrix}_{m \times l} \mathbf{C} = \begin{bmatrix} \mathbf{L}_1 \\ l \times l \\ \mathbf{L}_2 \\ (m-l) \times l \end{bmatrix}_{l \times l} \mathbf{T} = \begin{bmatrix} \mathbf{I} \\ l \times l \\ \mathbf{L}_2 \mathbf{L}_1^{-1} \\ (m-l) \times l \end{bmatrix}_{l \times l} \mathbf{A}_s. \quad (37)$$

For both the (36) and the (37), $\mathbf{\Pi}_r = \mathbf{I}(:, I)$ is a permutation submatrix corresponding to the l row skeletons indexed by $I \subset [m]$. With the row and column skeletons, the skeleton submatrix can be expressed as $\mathbf{A}_s = \mathbf{\Pi}_r^T \mathbf{C}$, and the corresponding row ID $\mathbf{C} = \mathbf{W} \mathbf{A}_s$ is exact. Therefore, for the CUR decomposition constructed with \mathbf{C} , $\mathbf{R} = \mathbf{A}(I, :)$, and $\mathbf{U} = \mathbf{C}^\dagger \mathbf{A} \mathbf{R}^\dagger$, (34) and (35) suggests that

$$\mathbf{CUR} = \mathbf{W} \mathbf{A}_s \mathbf{V}^T = \mathbf{C} \mathbf{C}^\dagger \mathbf{A}, \quad (38)$$

and therefore, $\|\mathbf{A} - \mathbf{CUR}\|_\xi = \|\mathbf{A} - \mathbf{C} \mathbf{C}^\dagger \mathbf{A}\|_\xi$, $\xi = 2, F$. That is, the CUR decomposition constructed with the CPQR based (Algorithm 5) or the LUPP based (Algorithm 6) row ID on \mathbf{C} is equivalent to the column ID with skeletons \mathbf{C} . In terms of the complexity, both the CPQR and the LUPP takes $O(ml^2)$ operations asymptotically. But in practice, the available implementations in benchmarks like the LAPACK for the LUPP is slightly more efficiently than those of the CPQR.

Alternatively, for the column selection with (randomized) DEIM (Algorithm 3), we can select the row skeletons by applying the DEIM on the leading left singular vectors or their randomized approximation $\mathbf{Q}\widehat{\mathbf{U}}$ (Algorithm 7). Specifically, [23] demonstrates that the CUR decomposition constructed with the DEIM point selection (Algorithm 2) on the exact leading k left and right singular vectors satisfies that

$$\|\mathbf{A} - \mathbf{CUR}\|_2 \leq (\eta_c + \eta_r) \sigma_{k+1}(\mathbf{A}).$$

where

$$\eta_c < \sqrt{\frac{mk}{3}} 2^k, \quad \eta_r < \sqrt{\frac{nk}{3}} 2^k$$

are asymptotically tight in the worst cases which are rare in practice. In terms of the complexity, the DEIM row selection takes $O(ml^2)$ more operations than the row selection with the LUPP on \mathbf{C} , but still runs in $O(ml^2)$ operations asymptotically.

Algorithm 5 Randomized CUR decomposition via CPQR

Input: $\mathbf{A} \in \mathbb{R}^{m \times n}$ with $m \geq n$, target rank $k < r = \text{rank}(\mathbf{A})$, sample size $\tilde{l} = k + O(1)$
Output: Indices of the rows skeletons $I \subset [m]$ and column skeletons $J \subset [n]$ such that $|I| = |J| = l$, $\mathbf{C} = \mathbf{A}(:, J) \in \mathbb{R}^{m \times l}$, $\mathbf{R} = \mathbf{A}(I, :) \in \mathbb{R}^{l \times n}$, $\mathbf{U} = \mathbf{C}^\dagger \mathbf{A} \mathbf{R}^\dagger \in \mathbb{R}^{l \times l}$

- 1: Apply Algorithm 1 on \mathbf{A} to select columns $\mathbf{C} = \mathbf{A}(:, J) \in \mathbb{R}^{m \times l}$
- 2: Apply an exact CPQR on \mathbf{C}^T (36) to select rows $I \subset [m]$, $|I| = l$ such that $\mathbf{R} = \mathbf{A}(I, :)$
- 3: Compute $\mathbf{U} = \mathbf{C}^\dagger \mathbf{A} \mathbf{R}^\dagger$ with a backward stable overdetermined least square solver

5 Single-view Interpolative and CUR Decomposition

The randomized pivoting based ID and CUR algorithms described above take at least two passes over the original matrix \mathbf{A} .⁵ The construction of the sketch for the skeleton selection takes

⁵Let us be careful here. Our new “poor man’s DEIM” can be executed as single pass, right? You extract Y , then do LUPP on Y directly, and use Y to build the interpolation matrix.

Algorithm 6 Randomized CUR decomposition via LUPP

Input: $\mathbf{A} \in \mathbb{R}^{m \times n}$ with $m \geq n$, target rank $k < r = \text{rank}(\mathbf{A})$, sample size $\tilde{l} = k + O(1)$
Output: Indices of the rows skeletons $I \subset [m]$ and column skeletons $J \subset [n]$ such that $|I| = |J| = l$, $\mathbf{C} = \mathbf{A}(:, J) \in \mathbb{R}^{m \times l}$, $\mathbf{R} = \mathbf{A}(I, :) \in \mathbb{R}^{l \times n}$, $\mathbf{U} = \mathbf{C}^\dagger \mathbf{A} \mathbf{R}^\dagger \in \mathbb{R}^{l \times l}$
1: Apply Algorithm 4 on \mathbf{A} to select columns $\mathbf{C} = \mathbf{A}(:, J) \in \mathbb{R}^{m \times l}$
2: Apply an exact LUPP on \mathbf{C}^T (37) to select rows $I \subset [m]$, $|I| = l$ such that $\mathbf{R} = \mathbf{A}(I, :)$
3: Compute $\mathbf{U} = \mathbf{C}^\dagger \mathbf{A} \mathbf{R}^\dagger$ with a backward stable overdetermined least square solver

Algorithm 7 Randomized CUR decomposition via DEIM

Input: $\mathbf{A} \in \mathbb{R}^{m \times n}$ with $m \geq n$, target rank $k < r = \text{rank}(\mathbf{A})$, sample size $\tilde{l} = k + O(1)$
Output: Indices of the rows skeletons $I \subset [m]$ and column skeletons $J \subset [n]$ such that $|I| = |J| = l$, $\mathbf{C} = \mathbf{A}(:, J) \in \mathbb{R}^{m \times l}$, $\mathbf{R} = \mathbf{A}(I, :) \in \mathbb{R}^{l \times n}$, $\mathbf{U} = \mathbf{C}^\dagger \mathbf{A} \mathbf{R}^\dagger \in \mathbb{R}^{l \times l}$
1: Apply Algorithm 3 on \mathbf{A} to select columns $\mathbf{C} = \mathbf{A}(:, J) \in \mathbb{R}^{m \times l}$, while returns $\mathbf{Q} \widehat{\mathbf{U}}$
2: Apply Algorithm 2 on $\mathbf{Q} \widehat{\mathbf{U}}$ to select rows $I \subset [m]$, $|I| = l$ such that $\mathbf{R} = \mathbf{A}(I, :)$
3: Compute $\mathbf{U} = \mathbf{C}^\dagger \mathbf{A} \mathbf{R}^\dagger$ with a backward stable overdetermined least square solver

one pass, while the explicit formation of $\mathbf{V}^T = \mathbf{C}^\dagger \mathbf{A}$ or $\mathbf{U} = \mathbf{C}^\dagger \mathbf{A} \mathbf{R}^\dagger$ with a least square solver requires another pass through \mathbf{A} . Although for the ID and the CUR decomposition, we are usually more interested in the skeletons than forming \mathbf{V} (in ID) and \mathbf{U} (in CUR) explicitly, the actual decomposition may be required in some cases, and is necessary for the posterior error evaluation.

However, revisiting \mathbf{A} may not be possible or affordable in certain circumstances. For instance, for a large-scale system that cannot be fitted in the core or a matrix that is stored implicitly in an oracle with non-trivial evaluation time, one pass over \mathbf{A} can be predominantly expensive, which makes revisiting infeasible. In this section, we briefly discuss the construction of the ID and the CUR decomposition in the single-view setting. That is, the original system \mathbf{A} is visited only once, and the order in which entries of \mathbf{A} are viewed cannot be specified.

Algorithm 8 Single-view column ID

Input: $\mathbf{A} \in \mathbb{R}^{m \times n}$ with $m \leq n$, target rank $k < r = \text{rank}(\mathbf{A}) = \min(m, n)$, sample size $\tilde{l} = k + O(1)$

Output: Column skeletons $J \subset [n]$, $|J| = l$, $\mathbf{C} = \mathbf{A}(:, J) \in \mathbb{R}^{m \times l}$, $\tilde{\mathbf{V}} \in \mathbb{R}^{n \times l}$

- 1: Select column skeletons with Algorithm 1 or 4
Output the skeleton indices $J \subset [n]$, the column sketch \mathbf{X} , and its corresponding pivoted QR or LU decomposition
- 2: Construct the approximation $\tilde{\mathbf{V}} = \mathbf{C} \mathbf{C}^\dagger \mathbf{T}^\dagger \mathbf{T} \mathbf{A} \approx \mathbf{C}^\dagger \mathbf{A}$ without revisiting \mathbf{A} :
 - (i) CPQR: for the CPQR, $\mathbf{X} \mathbf{\Pi} = \mathbf{Q} \begin{bmatrix} \mathbf{T}_1 & \mathbf{T}_2 \end{bmatrix}$,

$$\tilde{\mathbf{V}}^T := \begin{bmatrix} \mathbf{I} & \mathbf{T}_1^{-1} \mathbf{T}_2 \end{bmatrix} \mathbf{\Pi}^T = \mathbf{T}_1^{-1} \mathbf{Q}^T \mathbf{X}$$

$$\text{(ii) LUPP: for the LUPP, } \mathbf{X} \mathbf{\Pi} = \mathbf{T}^T \begin{bmatrix} \mathbf{L}_1^T & \mathbf{L}_2^T \end{bmatrix},$$

$$\tilde{\mathbf{V}}^T := \begin{bmatrix} \mathbf{I} & \mathbf{L}_1^{-T} \mathbf{L}_2^T \end{bmatrix} \mathbf{\Pi}^T = \mathbf{L}_1^{-T} \mathbf{T}^{-T} \mathbf{X}$$

Revisiting-free ID formation Without revisiting \mathbf{A} , Algorithm 8 construct the column ID $\mathbf{C} \tilde{\mathbf{V}}^T$ in a single view by approximating $\tilde{\mathbf{V}}^T$ based only on the sketch \mathbf{X} , in $O(nk^2)$ operations.

For the single-view setting, we assume that \mathbf{A} is full-rank and $m \leq n$, in contrast to the multiply-pass randomized setting where \mathbf{A} can be rank-deficient, and the subspace embedding is applied to the higher dimensional space ($m \geq n$) for the sake of efficiency.

Proposition 5.1. *For a full-rank matrix $\mathbf{A} \in \mathbb{R}^{m \times n}$ such that $m \leq n$, and an embedding dimension \tilde{l} such that $k + 4 \leq \tilde{l} \leq \text{rank}(\mathbf{A})$, let l be the rank of the column sketch $\mathbf{X} \in \mathbb{R}^{\tilde{l} \times n}$. Then, the rank- l column ID constructed with Algorithm 8 satisfies that,*

$$\|\mathbf{A} - \mathbf{C}\mathbf{V}^T\|_\xi \leq (\eta + 1) \cdot \|\mathbf{A}(\mathbf{I} - \mathbf{X}^\dagger \mathbf{X})\|_\xi, \quad (39)$$

where $\eta = \eta^{qr}$ or $\eta = \eta^{lu}$ depending on the pivoting scheme used, $\xi = 2, F$, and $\|\mathbf{A}(\mathbf{I} - \mathbf{X}^\dagger \mathbf{X})\|_\xi$ satisfies the set of expectation and tail bounds in Lemma 2.1.

Proof. By construction in Algorithm 8, $\tilde{\mathbf{V}}^T = (\mathbf{\Gamma}\mathbf{C})^\dagger \mathbf{X} = \mathbf{C}^\dagger \mathbf{\Gamma}^\dagger \mathbf{\Gamma}\mathbf{A}$. Therefore, we can bound the rank- l approximation error with the triangular inequality,

$$\begin{aligned} \|\mathbf{A} - \mathbf{C}\tilde{\mathbf{V}}^T\|_\xi &= \|(\mathbf{A} - \mathbf{C}\mathbf{C}^\dagger \mathbf{A}) + \mathbf{C}\mathbf{C}^\dagger(\mathbf{A} - \mathbf{\Gamma}^\dagger \mathbf{\Gamma}\mathbf{A})\|_\xi \\ &\leq \|\mathbf{A} - \mathbf{C}\mathbf{C}^\dagger \mathbf{A}\|_\xi + \|\mathbf{C}\mathbf{C}^\dagger\| \|\mathbf{A} - \mathbf{\Gamma}^\dagger \mathbf{\Gamma}\mathbf{A}\|_\xi \\ &\leq \eta \cdot \|\mathbf{A}(\mathbf{I} - \mathbf{X}^\dagger \mathbf{X})\|_\xi + \|\mathbf{A} - \mathbf{\Gamma}^\dagger \mathbf{\Gamma}\mathbf{A}\|_\xi. \end{aligned}$$

Since $\text{rank}(\mathbf{A}) = m \leq n$, we have $\mathbf{A}\mathbf{A}^\dagger = \mathbf{I}$. Meanwhile, with the definition of the pseudo-inverse $\mathbf{A}\mathbf{A}^\dagger \mathbf{A} = \mathbf{A}$, we have,

$$\|\mathbf{A} - \mathbf{A}\mathbf{X}^\dagger \mathbf{X}\|_\xi = \|\mathbf{A}\mathbf{A}^\dagger(\mathbf{A} - \mathbf{\Gamma}^\dagger \mathbf{\Gamma}\mathbf{A})\|_\xi = \|\mathbf{A} - \mathbf{\Gamma}^\dagger \mathbf{\Gamma}\mathbf{A}\|_\xi$$

Combining the equality and the inequality above gives (39). \square

We emphasize that the assumption $\text{rank}(\mathbf{A}) = m \leq n$ is necessary to maintain the upper bound of the rank- l approximation error $\|\mathbf{A} - \mathbf{C}\tilde{\mathbf{V}}^T\|_\xi$ for Algorithm 8. In specific, suppose $m > n$, then for an isotropic subspace embedding (i.e., $\mathbb{E} \mathbf{\Gamma}^\dagger \mathbf{\Gamma} = \mathbf{I}$), $(\mathbf{I} - \mathbf{\Gamma}^\dagger \mathbf{\Gamma})$ is an orthogonal projection onto a uniformly random dimension- $(m - l)$ subspace of \mathbb{R}^m . Therefore, $\mathbb{E} \|(\mathbf{I} - \mathbf{\Gamma}^\dagger \mathbf{\Gamma})\mathbf{A}\|_\xi = \frac{m-l}{r} \|\mathbf{A}\|_\xi$ for $m - l \leq r$, and $\|(\mathbf{I} - \mathbf{\Gamma}^\dagger \mathbf{\Gamma})\mathbf{A}\|_\xi \leq \|\mathbf{A}\|_\xi$ can be large, especially when $l \leq r \ll m$.

Single-view CUR Skeleton Selection To construct the CUR decomposition with pivoting in the single-view setting, we need to select the row and column skeletons simultaneously, in contrast to the multiple-pass circumstance where the skeletons are determined sequentially. To achieve this, we construct sketches for both the column and row spaces of \mathbf{A} , as shown in Algorithm 9.

In particular, when using the LUPP for pivoting, Algorithm 9 may fail when the row or the column sketches are rank deficient, $l_r < \tilde{l}$ or $l_c < \tilde{l}$. Nevertheless, for $\tilde{l} \ll r$, the sketches will be full-rank with high probability.

In addition, Algorithm 9 only selects the column and row skeletons in a single view, which is usually the main interest of the CUR decomposition, without explicitly constructing the middle matrix \mathbf{U} . With a restrictive assumption that \mathbf{A} is a square, full-rank matrix, the middle matrix \mathbf{U} can be approximated with the pivoted decompositions on the sketches \mathbf{X} and \mathbf{Y} , as in Algorithm 8, without revisiting \mathbf{A} , while satisfying Proposition 5.1. Otherwise

Algorithm 9 Single-view CUR skeleton selection

Input: $\mathbf{A} \in \mathbb{R}^{m \times n}$, target rank $k < r = \text{rank}(\mathbf{A})$, sample size $\tilde{l} = k + O(1)$

Output: Rows and column skeletons $I \subset [m]$, $|I| = l_r$, $J \subset [n]$, $|J| = l_c$, $\mathbf{R} = \mathbf{A}(I, :)$, $\mathbf{C} = \mathbf{A}(:, J)$

- 1: Draw oblivious subspace embeddings $\mathbf{\Gamma} \in \mathbb{R}^{\tilde{l} \times m}$ and $\mathbf{\Omega} \in \mathbb{R}^{\tilde{l} \times n}$
- 2: Construct the column sketch $\mathbf{X} = \mathbf{\Gamma} \mathbf{A}$ and the row sketch $\mathbf{Y} = \mathbf{A} \mathbf{\Omega}^T$ in a single pass
- 3: Apply the CPQR on \mathbf{X} or the row-wise LUPP on \mathbf{X}^T to identify $J \subseteq [n]$ where $|J| = l_c$
- 4: Apply the CPQR on \mathbf{Y}^T or the row-wise LUPP on \mathbf{X} to identify $I \subseteq [m]$ where $|I| = l_r$

when \mathbf{A} is rectangular or rank-deficient, such a revisiting-free approximation of \mathbf{U} may lead to a large approximation error, especially when \mathbf{A} admits a slow spectrum decay, or when $l \leq r \ll \min(m, n)$.

Meanwhile, if we are only interested in the row and column skeletons, then with small constant oversampling and $\mathbf{U} = \mathbf{C}^\dagger \mathbf{A} \mathbf{R}^\dagger$, the skeletons selected by Algorithm 9 enjoys the following performance guarantee.

Proposition 5.2. *For an embedding dimension \tilde{l} such that $k + 4 \leq \tilde{l} \leq \text{rank}(\mathbf{A})$, the low-rank CUR decomposition constructed with row and column skeletons, $\mathbf{C} \in \mathbb{R}^{m \times l_c}$ and $\mathbf{R} \in \mathbb{R}^{l_r \times n}$, selected by Algorithm 9, and $\mathbf{U} = \mathbf{C}^\dagger \mathbf{A} \mathbf{R}^\dagger$ satisfies that,*

$$\|\mathbf{A} - \mathbf{CUR}\|_\xi \leq \eta^c \cdot \|\mathbf{A}(\mathbf{I} - \mathbf{X}^\dagger \mathbf{X})\|_\xi + \eta^r \cdot \|\mathbf{(I} - \mathbf{Y} \mathbf{Y}^\dagger)\mathbf{A}\|_\xi, \quad (40)$$

where

$$\eta^c = \|\mathbf{I} - \mathcal{P}_X\| \leq \sqrt{1 + (n - l_c) \cdot 4^{l_c-1}}, \quad \eta^r = \|\mathbf{I} - \mathcal{P}_Y\| \leq \sqrt{1 + (m - l_r) \cdot 4^{l_r-1}}.$$

The exact values of η^c and η^r also depends on the pivoting scheme used. $\|\mathbf{A}(\mathbf{I} - \mathbf{X}^\dagger \mathbf{X})\|_\xi$ and $\|\mathbf{(I} - \mathbf{Y} \mathbf{Y}^\dagger)\mathbf{A}\|_\xi$ satisfy the set of expectation and tail bounds in Lemma 2.1.

Proof. The proof is adapted from [27], Lemma 3.1. In particular, let $\mathbf{C} \in \mathbb{R}^{m \times l_c}$ and $\mathbf{R} \in \mathbb{R}^{l_r \times n}$ be the column and row skeletons selected by Algorithm 9, respectively. We define the corresponding column and row ID approximation error, $\mathbf{A} = \mathbf{C} \mathbf{V}^T + \mathbf{E}$ and $\mathbf{A} = \mathbf{W} \mathbf{R} + \tilde{\mathbf{E}}$ such that,

$$\|\mathbf{E}\|_\xi \leq \eta^c \cdot \|\mathbf{A}(\mathbf{I} - \mathbf{X}^\dagger \mathbf{X})\|_\xi, \quad \|\tilde{\mathbf{E}}\|_\xi \leq \eta^r \cdot \|\mathbf{(I} - \mathbf{Y} \mathbf{Y}^\dagger)\mathbf{A}\|_\xi$$

Then with $\mathbf{U} = \mathbf{C}^\dagger \mathbf{A} \mathbf{R}^\dagger$, the residual of the CUR decomposition is given by

$$\mathbf{A} - \mathbf{CUR} = \mathbf{A} = \mathbf{C}(\mathbf{V}^T \mathbf{R}^\dagger) \mathbf{R} = \mathbf{A} - (\mathbf{A} - \mathbf{E}) \mathbf{R}^\dagger \mathbf{R} = (\mathbf{A} - \mathbf{A} \mathbf{R}^\dagger \mathbf{R}) + \mathbf{E} \mathbf{R}^\dagger \mathbf{R},$$

where

$$\mathbf{A} - \mathbf{A} \mathbf{R}^\dagger \mathbf{R} = \mathbf{A} - (\mathbf{W} \mathbf{R} + \tilde{\mathbf{E}}) \mathbf{R}^\dagger \mathbf{R} = (\mathbf{A} - \mathbf{W} \mathbf{R}) - \tilde{\mathbf{E}} \mathbf{R}^\dagger \mathbf{R} = \tilde{\mathbf{E}}(\mathbf{I} - \mathbf{R}^\dagger \mathbf{R}).$$

Therefore,

$$\mathbf{A} - \mathbf{CUR} = \tilde{\mathbf{E}}(\mathbf{I} - \mathbf{R}^\dagger \mathbf{R}) + \mathbf{E} \mathbf{R}^\dagger \mathbf{R}.$$

Then by the triangle inequality, since $\mathbf{R}^\dagger \mathbf{R}$ and $(\mathbf{I} - \mathbf{R}^\dagger \mathbf{R})$ are orthogonal projectors onto the space spanned by the row skeletons \mathbf{R} and its complement, we have

$$\|\mathbf{A} - \mathbf{CUR}\|_\xi = \|\tilde{\mathbf{E}}(\mathbf{I} - \mathbf{R}^\dagger \mathbf{R}) + \mathbf{E} \mathbf{R}^\dagger \mathbf{R}\|_\xi \leq \|\tilde{\mathbf{E}}(\mathbf{I} - \mathbf{R}^\dagger \mathbf{R})\|_\xi + \|\mathbf{E} \mathbf{R}^\dagger \mathbf{R}\|_\xi \leq \|\mathbf{E}\|_\xi + \|\tilde{\mathbf{E}}\|_\xi.$$

□

6 Numerical Experiments

In this section, we study the numerical performance of the described pivoting based randomized CUR algorithms from two perspectives:

1. accuracy measured by the rank- l approximation error $\|\mathbf{A} - \mathbf{CUR}\|_\xi$ for $\xi = 2$ or F , and
2. efficiency measured by the runtime scaling with respect to the rank parameter k .

As references, we compare performance of the pivoting based randomized CUR algorithms against that of some other methods for the CUR skeleton selection, including the leverage score sampling [11], and the spectrum-revealing CUR decomposition [29].

All experiments, except for those on the scaling of subspace embedding, are conducted in MATLAB R2020a. In the implementation, the computationally dominant procedures, including the matrix-matrix multiplication for sketching, the column pivoted QR, the LU with partial pivoting, and the SVD, are performed by either the MATLAB built-in functions. Meanwhile, the experiments on the scaling of subspace embedding with respect to the ambience dimension is conducted in Julia Version 1.5.3 with the JuliaMatrices/LowRankApprox.jl package [30].

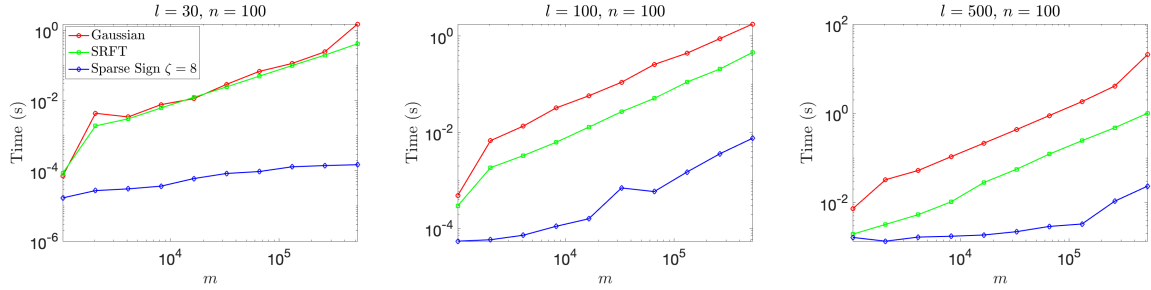


Figure 2: The runtime of applying different subspace embeddings $\mathbf{\Gamma} \in \mathbb{R}^{l \times m}$ to an arbitrary dense matrix of size $m \times n$, scaled with respect to the ambience dimension m , at different embedding dimension l and a fixed number of embeddings $n = 100$.

Stage 1: scaling of subspace embedding with the ambience dimension We start by comparing the runtime of applying various subspace embeddings $\mathbf{\Gamma} \in \mathbb{R}^{l \times m}$ to the column space of $\mathbf{A} \in \mathbb{R}^{m \times n}$, which can be interpreted as embedding n vectors in the ambience space \mathbb{R}^m to the lower dimensional space \mathbb{R}^l . We scale the experiments with respect to the ambience dimension m , at several different embedding dimension l , with a fixed number of repetitions $n = 1000$. Based on Figure 2, the sparse sign matrix enjoys a remarkable runtime advantage over the Gaussian embedding and the SRFT when m is moderate. The SRFT outperforms the Gaussian embedding in terms of efficiency, and such advantage is amplified as l increases.

Stage 2: scaling of pivoting based column selection with the problem size We now isolate and compare the runtime of different pivoting schemes in the greedy column selection stage (i.e., the second stage of the randomized pivoting based column selection), scaled with respect to the problem size n for different fixed ranks k . Specifically, the LUPP applies the LU with row pivoting on $\mathbf{X}^T \in \mathbb{R}^{n \times l}$. The CPQR runs the column pivoted QR over \mathbf{X}^T . The DEIM involves one orthonormalized power iteration, and the LU with row pivoting on an $n \times l$ matrix. In Figure 3, we can observe the considerable runtime advantage of the LUPP over the CPQR and DEIM, especially when l is sufficiently large.

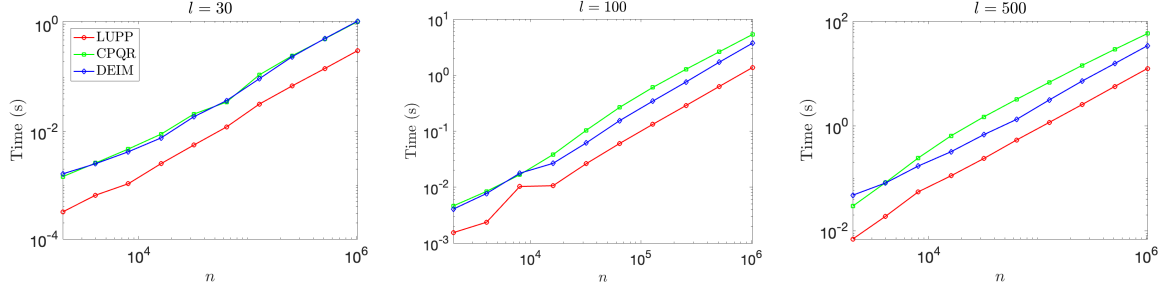


Figure 3: The runtime of various pivoting schemes on the sketches of size $n \times l$, scaled with respect to the problem size n , at different embedding dimension l .

Randomized CUR decompositions We test the CUR algorithms on a set of target matrices \mathbf{A} with various size and structure, including the synthetic random matrices with specific spectral patterns and some empirical data sets, as summarized below.

1. The **large** data set is a full-rank $4,282 \times 8,617$ sparse matrix with 20,635 nonzero entries. The matrix comes from a linear programming problem sequence.
2. The **YaleFace64x64** data set is a full-rank 165×4096 dense matrix, consisting of 165 face images each of size 64×64 . The flatten image vectors are centered and normalized such that the average image vector is zero, and the entries are bounded within $[-1, 1]$.
3. The **MNIST** training set consists of 60,000 images of hand-written digits from 0 to 9. Each image is of size 28×28 . The images are flatten and normalized to form a full-rank matrix of size $N \times d$ where N is the number of images and $d = 784$ is the size of the flatten images, with entries bounded in $[0, 1]$. The nonzero entries take approximately 20% of the matrix for both the training and the testing sets.
4. The *random sparse non-negative (SNN) matrix* is a category of random sparse matrices that is commonly used for testing the CUR algorithms, as introduced in [23], [27]. Given the dimension parameters (m, n) and a set of r sorted spectral parameters $s_1 \geq \dots \geq s_r > 0$, a random sparse non-negative matrix $\mathbf{A} \in \mathbb{R}^{m \times n}$ of rank- r takes the form,

$$\mathbf{A} = \text{SNN}\left(\{s_i\}_{i=1}^r; m, n\right) := \sum_{i=1}^r s_i \mathbf{x}_i \mathbf{y}_i^T \quad (41)$$

where $\mathbf{x}_i \in \mathbb{R}^m$, $\mathbf{y}_i \in \mathbb{R}^n$, $j \in [n]$ are random sparse vectors with non-negative entries. In the experiments, we construct two SNN matrices of distinct sizes. Specifically,

- (i) the **SNN1e3** is a 1000×1000 SNN matrix of rank $r = 1000$, with the spectral parameters $s_i = \frac{2}{i}$ for $i = 1, \dots, 100$ and $s_i = \frac{1}{i}$ for $i = 101, \dots, 1000$; and
- (ii) the **SNN1e6** is a $10^6 \times 10^6$ SNN matrix of rank $r = 400$, with the spectral parameters $s_i = \frac{2}{i}$ for $i = 1, \dots, 100$ and $s_i = \frac{1}{i}$ for $i = 101, \dots, 400$.

We compare the accuracy and efficiency of the following randomized CUR algorithms, scaled with respect to the rank of the approximation, on the matrices described above,

1. **Rand-CPQR, Rand-CPQR-1piter:** Randomized CUR decomposition via CPQR (with one power iteration) (Algorithm 5)
2. **Rand-LUPP, Rand-LUPP-1piter:** Randomized CUR decomposition via LUPP (with one power iteration) (Algorithm 6), [27],
3. **RSVD-DEIM:** Randomized CUR decomposition via DEIM (Algorithm 7),
4. **RSVD-LS:** Randomize rank- k SVD [12], followed by the leverage score sampling [11],
5. **srcur:** Spectrum-revealing CUR decomposition [29].

In all the algorithms, we use the Gaussian matrices as the subspace embedding.

We point out that, in the above figures, we compare the approximation errors of the rank- k

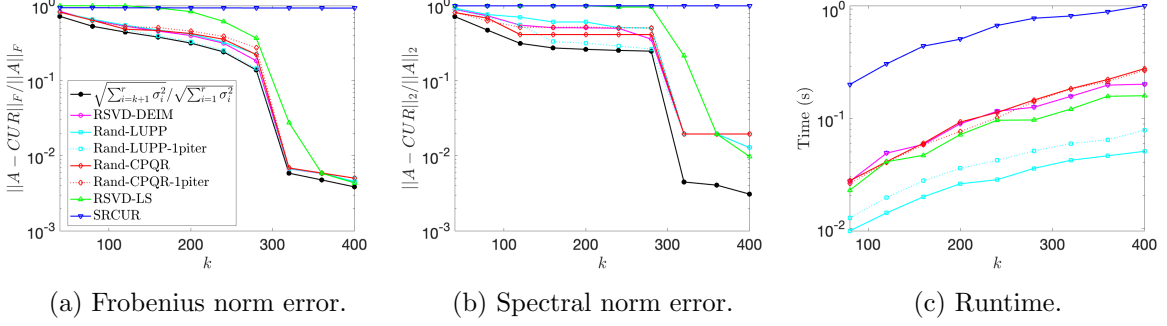


Figure 4: Relative error and runtime of randomized CUR on the **large** data set.

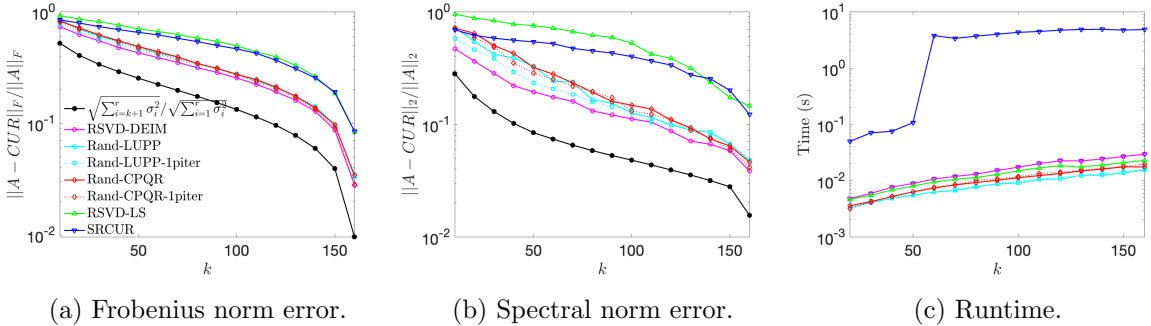


Figure 5: Relative error and runtime of randomized CUR on the **YaleFace64x64** data set.

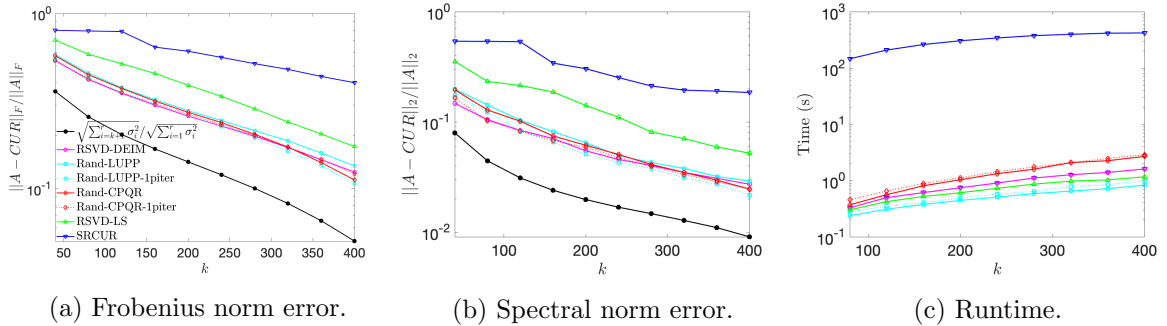


Figure 6: Relative error and runtime of randomized CUR on the training set of **MNIST**.

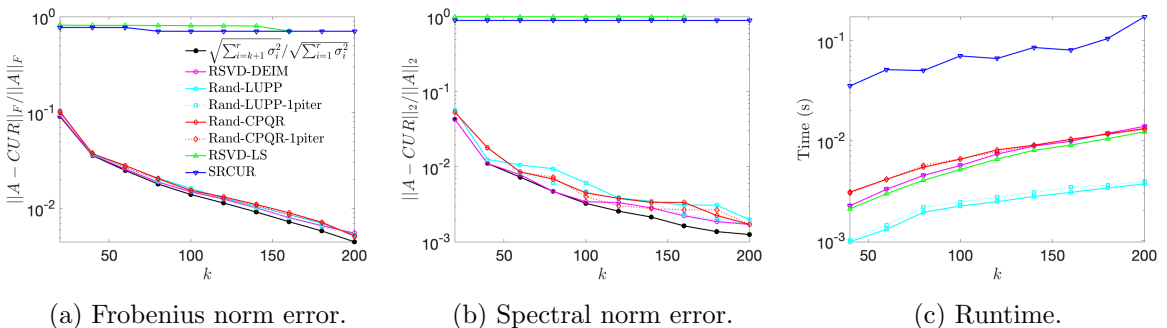


Figure 7: Relative error and runtime of randomized CUR on a 1000×1000 sparse non-negative random matrix, **SNN1e3**.

CUR decompositions (i.e., without oversampling) to the optimal rank- k approximation error $\|\mathbf{A} - \mathbf{A}_k\|_\xi$ as a lower bound only for the reference purpose. While in practice, as illustrated

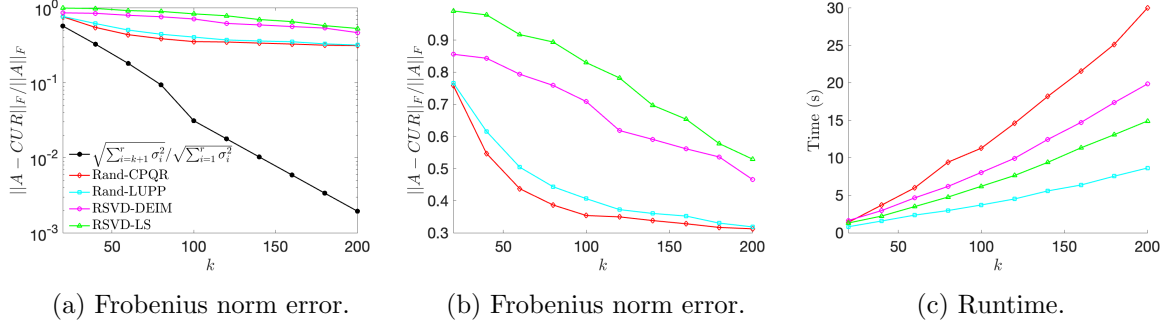


Figure 8: Relative error and runtime of randomized CUR on a $10^6 \times 10^6$ sparse non-negative random matrix, **SNN1e6**.

in the above sections, we usually construct the randomized CUR decompositions with small constant oversampling (e.g., $l - k = 5$ or 10) to achieve the desired accuracy.

From Figure 4–7, we observe that all the pivoting based randomized CUR algorithms share the similar approximation accuracy, and enjoy considerably lower approximation error than the leverage score sampling and the spectrum-revealing CUR (SRCUR) with the same rank. In terms of the efficiency, the Rand-LUPP demonstrates the most appreciable runtime among all the algorithms, especially when \mathbf{A} is sparse. Meanwhile, we observe that, for both the Rand-CPQR and Rand-LUPP, constructing the sketches with one plain power iteration can observably improve the accuracy, without sacrificing the efficiency significantly. In Figure 8, the similar performance is also observed on the synthetic large-scale problem, **SNN1e6**, where the matrix is only accessible as a fast matrix-vector multiplication (matvec) oracle such that each matvec takes $o(mn)$ (i.e., $O((m+n)r)$ in our construction) operations. It is worth to notice that, as Lemma 3.2 and 3.3 suggest, the accuracy of the CUR decomposition comparing to the optimal approximation of the same rank is degraded significantly as $m, n \gg k$. Nevertheless, on the synthetic large-scale problem, the Rand-LUPP still enjoys the favorable efficiency, while maintaining competitive accuracy.

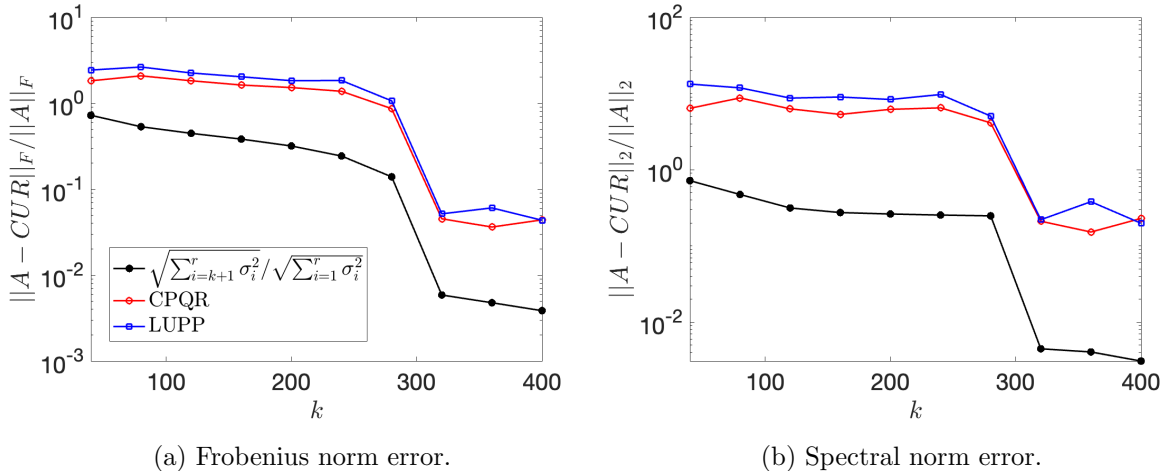


Figure 9: Relative error and runtime of the single-view column ID on the **large** data set.

Single-view pivoting based column ID Figure 9 compares the approximation accuracy of the low-rank single-view column ID (Algorithm 8) with the revisiting-free \mathbf{V} approximation on the **large** data set (since the matrix is full rank, while m and n share the same order of

magnitude). We can observe that in contrast to that of the column ID with $\mathbf{V}^T = \mathbf{C}^\dagger \mathbf{A}$, the error of the revisiting-free approximation does not necessarily decrease monotonically as the rank k increases. Meanwhile, pivoting with the CPQR enjoys slightly better accuracy than pivoting with the LUPP. Despite the observably larger approximation error comparing to the column ID with $\mathbf{V}^T = \mathbf{C}^\dagger \mathbf{A}$, the revisiting-free column ID converges well with respect to the increasing rank k . That is, with sufficient oversampling, the revisiting-free column ID provides a good low-rank approximation for \mathbf{A} . For instance, Figure 9 suggests that, for the `large` data set, a rank- l revisiting-free column ID with $l \geq 400$ is necessary to achieve a good approximation of \mathbf{A}_k with $k = 200$, which corresponds to a $O(k)$ oversampling.

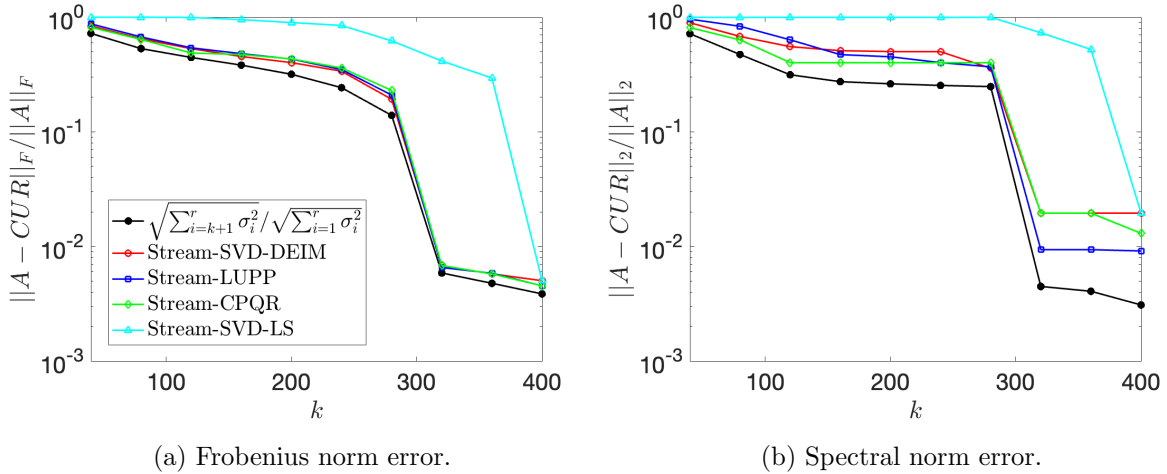


Figure 10: Relative error and runtime of the single-view CUR on the `large` data set.

Single-view CUR skeletons selections with $\mathbf{U} = \mathbf{C}^\dagger \mathbf{A} \mathbf{R}^\dagger$ Now we compare the approximation accuracy of the CUR decomposition with the pivoting based single-view skeleton selection and $\mathbf{U} = \mathbf{C}^\dagger \mathbf{A} \mathbf{R}^\dagger$:

1. **Stream-CPQR**: Single-view CUR skeleton selection via CPQR (Algorithm 9 with CPQR),
2. **Stream-LUPP**: Single-view CUR skeleton selection via LUPP (Algorithm 9 with LUPP),
3. **Stream-SVD-DEIM**: Single-view rank- k SVD [28], followed by the DEIM point selection on the approximations of left and right singular vectors,
4. **Stream-SVD-LS**: Single-view rank- k SVD [28], followed by leverage score sampling [11].

As in the multiple-pass circumstance, we scale with respect to the approximation rank, use the Gaussian matrices for subspace embedding, and compare against the optimal rank- k approximation error without oversampling.

Figure 10 suggests that, as in the multiple-pass setting, with both the CPQR and the LUPP, the pivoting based randomized skeleton selection procedures provide nearly optimal column and row skeleton sets for the CUR decomposition in the single-view setting.

7 Conclusions

The pivoting based randomized CUR decomposition consists of two stages. The first stage constructs a low-rank decomposition of \mathbf{A} with the subspace embedding. The second stage applies classical pivoting schemes to the low-dimensional representation of \mathbf{A} obtained in the first stage, and selects the skeletons greedily. We have provided a brief overview of some common subspace embeddings, along with the construction of sketches and low-rank decompositions for

the first stage. For the second stage, we review two classical pivoting schemes, namely the column pivoted QR (CPQR) and the LU with partial pivoting (LUPP). We present several skeleton selection procedures as different combinations of the low-rank decomposition (the first stage) and the pivoting scheme (the second stage). Starting with two popular randomized skeleton selection algorithms based on the CPQR and the DEIM, we merge the components of the two with appreciable efficiency and propose a simple randomized skeleton selection procedure based on the LUPP. We also analyze the approximation error of the low-rank column interpolative decomposition (ID) with skeleton columns selected by these randomized pivoting schemes. Then, we generalize the column selection to the two-sided skeleton selection and the CUR decomposition. In addition, we briefly discuss the construction of the low-rank ID and the CUR skeleton selection in the single-view (or “streaming”) setting. The empirical performance of the CUR skeleton selection algorithms suggests that the LUPP is a more efficient pivoting scheme than the CPQR and the DEIM for the greedy skeleton selection, while maintaining similar approximation accuracy for the skeleton sets selected.

References

- [1] C. Eckart and G. Young, “The approximation of one matrix by another of lower rank,” *Psychometrika*, vol. 1, no. 3, pp. 211–218, Sep. 1936, ISSN: 1860-0980. DOI: [10.1007/BF02288367](https://doi.org/10.1007/BF02288367). [Online]. Available: <https://doi.org/10.1007/BF02288367>.
- [2] A. F. Ruston, “Auerbach’s theorem and tensor products of banach spaces,” *Mathematical Proceedings of the Cambridge Philosophical Society*, vol. 58, no. 3, pp. 476–480, 1962. DOI: [10.1017/S0305004100036744](https://doi.org/10.1017/S0305004100036744).
- [3] L. N. Trefethen and R. S. Schreiber, “Average-case stability of gaussian elimination,” *SIAM Journal on Matrix Analysis and Applications*, vol. 11, no. 3, pp. 335–360, 1990. DOI: [10.1137/0611023](https://doi.org/10.1137/0611023). eprint: <https://doi.org/10.1137/0611023>. [Online]. Available: <https://doi.org/10.1137/0611023>.
- [4] M. Gu and S. C. Eisenstat, “Efficient algorithms for computing a strong rank-revealing qr factorization,” *SIAM Journal on Scientific Computing*, vol. 17, no. 4, pp. 848–869, 1996. DOI: [10.1137/0917055](https://doi.org/10.1137/0917055). eprint: <https://doi.org/10.1137/0917055>. [Online]. Available: <https://doi.org/10.1137/0917055>.
- [5] S. Goreinov, E. Tyrtyshnikov, and N. Zamarashkin, “A theory of pseudoskeleton approximations,” *Linear Algebra and its Applications*, vol. 261, no. 1, pp. 1–21, 1997, ISSN: 0024-3795. DOI: [https://doi.org/10.1016/S0024-3795\(96\)00301-1](https://doi.org/10.1016/S0024-3795(96)00301-1). [Online]. Available: <https://www.sciencedirect.com/science/article/pii/S0024379596003011>.
- [6] P. Indyk and R. Motwani, “Approximate nearest neighbors: Towards removing the curse of dimensionality,” in *Proceedings of the Thirtieth Annual ACM Symposium on Theory of Computing*, ser. STOC ’98, Dallas, Texas, USA: Association for Computing Machinery, 1998, pp. 604–613, ISBN: 0897919629. DOI: [10.1145/276698.276876](https://doi.org/10.1145/276698.276876). [Online]. Available: <https://doi.org/10.1145/276698.276876>.
- [7] R. Baraniuk, M. Davenport, R. DeVore, and M. Wakin, “A simple proof of the restricted isometry property for random matrices,” *Constructive Approximation*, vol. 28, no. 3, pp. 253–263, Dec. 2008, ISSN: 1432-0940. DOI: [10.1007/s00365-007-9003-x](https://doi.org/10.1007/s00365-007-9003-x). [Online]. Available: <https://doi.org/10.1007/s00365-007-9003-x>.

[8] V. Rokhlin and M. Tygert, “A fast randomized algorithm for overdetermined linear least-squares regression,” *Proceedings of the National Academy of Sciences*, vol. 105, no. 36, pp. 13 212–13 217, 2008, ISSN: 0027-8424. DOI: [10.1073/pnas.0804869105](https://doi.org/10.1073/pnas.0804869105). eprint: <https://www.pnas.org/content/105/36/13212.full.pdf>. [Online]. Available: <https://www.pnas.org/content/105/36/13212>.

[9] F. Woolfe, E. Liberty, V. Rokhlin, and M. Tygert, “A fast randomized algorithm for the approximation of matrices,” *Applied and Computational Harmonic Analysis*, vol. 25, no. 3, pp. 335–366, 2008, ISSN: 1063-5203. DOI: <https://doi.org/10.1016/j.acha.2007.12.002>. [Online]. Available: <https://www.sciencedirect.com/science/article/pii/S1063520307001364>.

[10] A. Çivril and M. Magdon-Ismail, “On selecting a maximum volume sub-matrix of a matrix and related problems,” *Theoretical Computer Science*, vol. 410, no. 47, pp. 4801–4811, 2009, ISSN: 0304-3975. DOI: <https://doi.org/10.1016/j.tcs.2009.06.018>. [Online]. Available: <https://www.sciencedirect.com/science/article/pii/S0304397509004101>.

[11] M. W. Mahoney and P. Drineas, “Cur matrix decompositions for improved data analysis,” *Proceedings of the National Academy of Sciences*, vol. 106, no. 3, pp. 697–702, 2009, ISSN: 0027-8424. DOI: [10.1073/pnas.0803205106](https://doi.org/10.1073/pnas.0803205106). eprint: <https://www.pnas.org/content/106/3/697.full.pdf>. [Online]. Available: <https://www.pnas.org/content/106/3/697>.

[12] N. Halko, P. G. Martinsson, and J. A. Tropp, “Finding structure with randomness: Probabilistic algorithms for constructing approximate matrix decompositions,” *SIAM Review*, vol. 53, no. 2, pp. 217–288, 2011. DOI: [10.1137/090771806](https://doi.org/10.1137/090771806). eprint: <https://doi.org/10.1137/090771806>. [Online]. Available: <https://doi.org/10.1137/090771806>.

[13] J. A. TROPP, “Improved analysis of the subsampled randomized hadamard transform,” *Advances in Adaptive Data Analysis*, vol. 03, no. 01n02, pp. 115–126, 2011. DOI: [10.1142/S1793536911000787](https://doi.org/10.1142/S1793536911000787). eprint: <https://doi.org/10.1142/S1793536911000787>. [Online]. Available: <https://doi.org/10.1142/S1793536911000787>.

[14] P. Drineas, M. Magdon-Ismail, M. W. Mahoney, and D. P. Woodruff, “Fast approximation of matrix coherence and statistical leverage,” *J. Mach. Learn. Res.*, vol. 13, no. 1, pp. 3475–3506, Dec. 2012, ISSN: 1532-4435.

[15] C. Boutsidis and A. Gittens, “Improved matrix algorithms via the subsampled randomized hadamard transform,” *SIAM Journal on Matrix Analysis and Applications*, vol. 34, no. 3, pp. 1301–1340, 2013. DOI: [10.1137/120874540](https://doi.org/10.1137/120874540). eprint: <https://doi.org/10.1137/120874540>. [Online]. Available: <https://doi.org/10.1137/120874540>.

[16] J. Kurzak, P. Luszczek, M. Faverge, and J. Dongarra, “Lu factorization with partial pivoting for a multicore system with accelerators,” *IEEE Transactions on Parallel and Distributed Systems*, vol. 24, no. 8, pp. 1613–1621, 2013. DOI: [10.1109/TPDS.2012.242](https://doi.org/10.1109/TPDS.2012.242).

[17] X. Meng and M. W. Mahoney, “Low-distortion subspace embeddings in input-sparsity time and applications to robust linear regression,” in *Proceedings of the Forty-Fifth Annual ACM Symposium on Theory of Computing*, ser. STOC ’13, Palo Alto, California, USA: Association for Computing Machinery, 2013, pp. 91–100, ISBN: 9781450320290. DOI: [10.1145/2488608.2488621](https://doi.org/10.1145/2488608.2488621). [Online]. Available: <https://doi.org/10.1145/2488608.2488621>.

[18] J. Nelson and H. L. Nguyn, “Osnap: Faster numerical linear algebra algorithms via sparser subspace embeddings,” in *2013 IEEE 54th Annual Symposium on Foundations of Computer Science*, 2013, pp. 117–126. DOI: [10.1109/FOCS.2013.21](https://doi.org/10.1109/FOCS.2013.21).

[19] C. Boutsidis and D. P. Woodruff, “Optimal cur matrix decompositions,” in *Proceedings of the Forty-Sixth Annual ACM Symposium on Theory of Computing*, ser. STOC ’14, New York, New York: Association for Computing Machinery, 2014, pp. 353–362, ISBN: 9781450327107. DOI: [10.1145/2591796.2591819](https://doi.org/10.1145/2591796.2591819). [Online]. Available: <https://doi.org/10.1145/2591796.2591819>.

[20] D. P. Woodruff, “Sketching as a tool for numerical linear algebra,” *Found. Trends Theor. Comput. Sci.*, vol. 10, no. 1–2, pp. 1–157, Oct. 2014, ISSN: 1551-305X. DOI: [10.1561/0400000060](https://doi.org/10.1561/0400000060). [Online]. Available: <https://doi.org/10.1561/0400000060>.

[21] M. B. Cohen, “Nearly tight oblivious subspace embeddings by trace inequalities,” in *Proceedings of the Twenty-Seventh Annual ACM-SIAM Symposium on Discrete Algorithms*, ser. SODA ’16, Arlington, Virginia: Society for Industrial and Applied Mathematics, 2016, pp. 278–287, ISBN: 9781611974331.

[22] Z. Drmač and S. Gugercin, “A new selection operator for the discrete empirical interpolation method—improved a priori error bound and extensions,” *SIAM Journal on Scientific Computing*, vol. 38, no. 2, A631–A648, 2016. DOI: [10.1137/15M1019271](https://doi.org/10.1137/15M1019271). eprint: <https://doi.org/10.1137/15M1019271>. [Online]. Available: <https://doi.org/10.1137/15M1019271>.

[23] D. C. Sorensen and M. Embree, “A deim induced cur factorization,” *SIAM Journal on Scientific Computing*, vol. 38, no. 3, A1454–A1482, 2016. DOI: [10.1137/140978430](https://doi.org/10.1137/140978430). eprint: <https://doi.org/10.1137/140978430>. [Online]. Available: <https://doi.org/10.1137/140978430>.

[24] D. Anderson and M. Gu, “An efficient, sparsity-preserving, online algorithm for low-rank approximation,” in *Proceedings of the 34th International Conference on Machine Learning - Volume 70*, ser. ICML’17, Sydney, NSW, Australia: JMLR.org, 2017, pp. 156–165.

[25] K. L. Clarkson and D. P. Woodruff, “Low-rank approximation and regression in input sparsity time,” *J. ACM*, vol. 63, no. 6, Jan. 2017, ISSN: 0004-5411. DOI: [10.1145/3019134](https://doi.org/10.1145/3019134). [Online]. Available: <https://doi.org/10.1145/3019134>.

[26] J. A. Tropp, A. Yurtsever, M. Udell, and V. Cevher, “Fixed-rank approximation of a positive-semidefinite matrix from streaming data,” in *Advances in Neural Information Processing Systems*, I. Guyon, U. V. Luxburg, S. Bengio, H. Wallach, R. Fergus, S. Vishwanathan, and R. Garnett, Eds., vol. 30, Curran Associates, Inc., 2017. [Online]. Available: <https://proceedings.neurips.cc/paper/2017/file/4558dbb6f6f8bb2e16d03b85bde76e2c-Paper.pdf>.

[27] S. Voronin and P.-G. Martinsson, “Efficient algorithms for cur and interpolative matrix decompositions,” *Advances in Computational Mathematics*, vol. 43, no. 3, pp. 495–516, Jun. 2017, ISSN: 1572-9044. DOI: [10.1007/s10444-016-9494-8](https://doi.org/10.1007/s10444-016-9494-8). [Online]. Available: <https://doi.org/10.1007/s10444-016-9494-8>.

[28] J. A. Tropp, A. Yurtsever, M. Udell, and V. Cevher, “Streaming low-rank matrix approximation with an application to scientific simulation,” *SIAM Journal on Scientific Computing*, vol. 41, no. 4, A2430–A2463, 2019. DOI: [10.1137/18M1201068](https://doi.org/10.1137/18M1201068). eprint: <https://doi.org/10.1137/18M1201068>. [Online]. Available: <https://doi.org/10.1137/18M1201068>.

[29] C. Chen, M. Gu, Z. Zhang, W. Zhang, and Y. Yu, “Efficient spectrum-revealing cur matrix decomposition,” in *Proceedings of the Twenty Third International Conference on Artificial Intelligence and Statistics*, S. Chiappa and R. Calandra, Eds., ser. Proceedings of Machine Learning Research, vol. 108, PMLR, 26–28 Aug 2020, pp. 766–775. [Online]. Available: <http://proceedings.mlr.press/v108/chen20a.html>.

[30] K. Ho, S. Olver, T. Kelman, E. Jarlebring, J. TagBot, and M. Slevinsky, *Lowrankapprox.jl*: V0.4.3, <https://github.com/JuliaMatrices/LowRankApprox.jl>, 2020.

- [31] P.-G. Martinsson and J. A. Tropp, “Randomized numerical linear algebra: Foundations and algorithms,” *Acta Numerica*, vol. 29, pp. 403–572, 2020. DOI: [10.1017/S0962492920000021](https://doi.org/10.1017/S0962492920000021).
- [32] M. Dereziński and M. Mahoney, “Determinantal point processes in randomized numerical linear algebra,” *Notices of the American Mathematical Society*, vol. 68, p. 1, Jan. 2021. DOI: [10.1090/noti2202](https://doi.org/10.1090/noti2202).

A DEIM versus LU with partial pivoting (LUPP)

We will show that the DEIM point selection is equivalent to the LU with row pivoting, in the sense that they provide the same ordering of rows.

Claim A.1 (Equivalence between DEIM and LUPP). *For $\mathbf{V} \in \mathbb{R}^{n \times k}$, let $\mathbf{q} = \text{DEIM}(\mathbf{V}) \in [n]^k$ be the sequence of skeleton indices selected by Algorithm 2. Meanwhile, let $\mathbf{p} \in [n]^k$ be the sequence of rows pivoted in the LU decomposition with partial (row) pivoting of \mathbf{V} ,*

$$\hat{\mathbf{P}}^T \mathbf{V} = \hat{\mathbf{L}} \mathbf{U},$$

where $\hat{\mathbf{P}} = \mathbf{I}(:, \mathbf{p}) \in \mathbb{R}^{n \times k}$, $\hat{\mathbf{L}}, \mathbf{U} \in \mathbb{R}^{k \times k}$ lower and upper triangular, respectively. Then $\mathbf{p} = \mathbf{q}$. That is, the DEIM selects skeleton points in the same order as the LUPP choices pivots.

Proof. We denote the following:

- $\mathbf{P} \in \mathbb{R}^{n \times n}$ a permutation such that $\mathbf{P}(:, 1 : k) = \hat{\mathbf{P}} = \mathbf{I}(:, \mathbf{p})$, where $\mathbf{p} = [i_1, \dots, i_k] \subset [n]$,
- $\mathbf{p}_j = [i_1, \dots, i_j]$, $\mathbf{P}_j = \mathbf{I}(:, \mathbf{p}_j) \in \mathbb{R}^{n \times j}$,
- $\mathbf{V} = [\mathbf{v}_1, \dots, \mathbf{v}_k] \in \mathbb{R}^{n \times k}$ and $\mathbf{V}_j = [\mathbf{v}_1, \dots, \mathbf{v}_j]$,
- $\mathbf{L} \in \mathbb{R}^{n \times k}$ such that $\mathbf{L}(1 : k, :) \in \mathbb{R}^{k \times k}$ is lower triangular,
- $\mathbf{U} \in \mathbb{R}^{k \times k}$ is invertible and upper triangular with diagonal entries equal to 1.

At the $(j + 1)$ -th iteration, Algorithm 2 computes the residue,

$$\mathbf{r}_{j+1} = \mathbf{v}_{j+1} - \mathbf{V}_j (\mathbf{P}_j^T \mathbf{V}_j)^{-1} \mathbf{P}_j^T \mathbf{v}_{j+1}. \quad (42)$$

We can first make a simple observation that,

$$\mathbf{P}_j^T \mathbf{r}_{j+1} = \mathbf{P}_j^T \mathbf{v}_{j+1} - (\mathbf{P}_j^T \mathbf{V}_j) (\mathbf{P}_j^T \mathbf{V}_j)^{-1} \mathbf{P}_j^T \mathbf{v}_{j+1} = \mathbf{0} \quad (43)$$

Just as the LUPP, in each step, the DEIM zeroes-out previously selected indices in the residue and selects the next index with the maximum absolute residue. Then $\mathbf{p} = \mathbf{q}$ follows by induction.

To show the equivalence between the LUPP and DEIM, we demonstrate that there exist lower and upper triangular matrices \mathbf{L} and \mathbf{U} as described such that $\mathbf{P}^T \mathbf{V} = \mathbf{L} \mathbf{U}$. Consider $\mathbf{L} = \mathbf{P}^T \mathbf{R}$ where $\mathbf{R} = [\mathbf{r}_1, \dots, \mathbf{r}_k]$ with $\mathbf{r}_1 = \mathbf{v}_1$, and for all $j \in [k - 1]$, \mathbf{r}_{j+1} is given by (42). Then (43) indicates that $\mathbf{L}(1 : k, :)$ is lower triangular as desired. Now we want to find $\mathbf{U} \in \mathbb{R}^{k \times k}$ such that $\mathbf{P}^T \mathbf{V} = \mathbf{P}^T \mathbf{R} \mathbf{U}$. It is sufficient to find such \mathbf{U} that $\mathbf{R} = \mathbf{V} \mathbf{U}^{-1}$. By considering the $(j + 1)$ -th column of \mathbf{R} , we can observe that,

$$\mathbf{r}_{j+1} = [\mathbf{V}_j, \mathbf{v}_{j+1}] \begin{bmatrix} \mathbf{w}_j \\ \vdots \\ 1 \end{bmatrix} = \mathbf{V} \begin{bmatrix} \mathbf{w}_j \\ \vdots \\ 1 \end{bmatrix}$$

where $\mathbf{w}_j := (\mathbf{P}_j^T \mathbf{V}_j)^{-1} \mathbf{P}_j^T \mathbf{v}_{j+1} \in \mathbb{R}^j$. Therefore, we can construct,

$$\mathbf{U}^{-1} = \begin{bmatrix} 1 & w_1 & \cdots & & \cdots & & \\ 0 & 1 & \cdots & \mathbf{w}_j & \cdots & & \\ \vdots & 0 & \ddots & & \cdots & \mathbf{w}_{k-1} & \\ \vdots & \vdots & 0 & 1 & \cdots & & \\ \vdots & \vdots & \vdots & 0 & \ddots & & \\ \vdots & \vdots & \vdots & \vdots & 0 & 1 & \end{bmatrix}$$

such that the inverse $\mathbf{U} \in \mathbb{R}^{k \times k}$ is upper triangular with diagonal entries equal to 1. \square

B LUPP on Gaussian Sample Matrices: Average Cases

The upper bounds on η^{lu} in the worst case for an arbitrary sketch \mathbf{X} in (29) is asymptotically tight. That is, there exists an artificial $\mathbf{X}^T \in \mathbb{R}^{n \times l}$ where the partially pivoted LU decomposition results in an \mathbf{L} with $\max_{ij} \left| \left(\mathbf{L}_2 \mathbf{L}_1^{-1} \right)_{ij} \right|$ depending exponentially on l . In particular, we consider the following matrix,

$$\mathbf{L} = \begin{bmatrix} 1 & & & \\ -1 & 1 & & \\ \vdots & \ddots & \ddots & \\ -1 & \dots & -1 & 1 \\ 1 & \dots & 1 & 1 \\ \vdots & & \vdots & \vdots \\ 1 & \dots & 1 & 1 \end{bmatrix},$$

with $L_{jj} = 1$ for $1 \leq j \leq l$, $L_{ij} = -1$ for $1 \leq j < i \leq l$, and $L_{ij} = 1$ wherever $l+1 \leq i \leq m$. Based the forward substitution steps in (30), we have,

$$\left(\mathbf{L}_2 \mathbf{L}_1^{-1} \right)_{ij} = 2^{l-j}, \quad \forall 1 \leq i \leq m-l, \quad 1 \leq j \leq l,$$

and therefore $\max_{ij} \left| \left(\mathbf{L}_2 \mathbf{L}_1^{-1} \right)_{ij} \right| = 2^{l-1}$.

In spite of the exponential dependency on l in the worst scenario, η^{lu} grows much slower with respect to l in practice. The average-case analysis on the stability of the pivoted Gaussian elimination in [3] supports such empirical observation. In specific, [3] demonstrates that, for $l \leq 1024$, the LU with partial pivoting on an $l \times l$ Gaussian random matrix results in an upper triangular matrix $\mathbf{U} \in \mathbb{R}^{l \times l}$ such that $\langle \max_{ij} |U_{ij}| \rangle \lesssim l^{2/3}$ in the average case.

We denote the columns of $\mathbf{A} \in \mathbb{R}^{m \times n}$ as $\mathbf{a}_j = \mathbf{A}(:, j)$ for all $j = 1, \dots, n$. Then with a Gaussian embedding $\mathbf{\Gamma} \in \mathbb{R}^{l \times m}$ with $\Gamma_{ij} \sim \mathcal{N}(0, 1/l)$, we have $\mathbf{X} = \mathbf{\Gamma} \mathbf{A}$ such that $X_{ij} \sim \mathcal{N}(0, \|\mathbf{a}_j\|^2/l)$ for all $j = 1, \dots, l$. In particular, the rows $\{\mathbf{X}(i, :) : i = 1, \dots, l\}$ are independent, but the columns $\{\mathbf{X}(:, j) : j = 1, \dots, n\}$ are dependent. By defining a diagonal matrix $\mathbf{D} = \text{diag}(\|\mathbf{a}_1\|/\sqrt{l}, \dots, \|\mathbf{a}_n\|/\sqrt{l}) \in \mathbb{R}^{n \times n}$, we have $\mathbf{X}^T = \mathbf{D} \mathbf{G}$ where $\mathbf{G} \in \mathbb{R}^{n \times l}$ is a full-rank matrix whose columns are dependent standard Gaussian random vectors.

Now we make two observations on the growth of

$$\rho \triangleq \max_{ij} \left| \left(\mathbf{L}_2 \mathbf{L}_1^{-1} \right)_{ij} \right|$$

in the average cases. From the forward substitution steps (30), we know that ρ tends to increase more rapidly when $|L_{ij}| \approx 1$. While for the partially pivoted LU,

$$L_{ij} = \frac{X_{ji}^{(j-1)}}{X_{ii}^{(j-1)}}, \quad \left| X_{ii}^{(j-1)} \right| = \max_{j \leq t \leq n} \left| X_{jt}^{(j-1)} \right|, \quad 1 \leq j \leq l, \quad j \leq i \leq n,$$

where $\mathbf{X}^{(j-1)}$ denotes the modified matrix of \mathbf{X} after $(j-1)$ steps of pivoted Gaussian elimination and the j -th row pivoting. Therefore, we first observe that ρ is expected to grow faster with

respect to l when $\{|X_{ji}| : 1 \leq i \leq n, 1 \leq j \leq l\}$ are tightly distributed. That is, $\mathbf{D} \approx \mathbf{I}$. Now we suppose $\mathbf{D} = \mathbf{I}$, since each column of \mathbf{X} is a standard Gaussian random vector, our second observation is that ρ tends to grow faster when the l pivoted columns of \mathbf{X} are approximately orthogonal. This is because the Gaussian elimination on a nearly orthogonal set of rows introduces little perturbation to the distribution of the row norms, and therefore the distribution of the entry-wise absolute values $|X_{ji}|$, given that the $\{X_{ji} : j = 1, \dots, l\}$ are independent. Therefore, starting with $|X_{ji}|$ tightly distributed, the approximate orthogonality of the l pivoted columns in \mathbf{X} leads to $|L_{ij}| \approx 1$ as j increases. With these observations, we reduce the problem of determining an upper bound of ρ for \mathbf{X} of an arbitrary matrix \mathbf{A} , to the problem of estimating ρ for a Gaussian random matrix $\mathbf{G} \in \mathbb{R}^{n \times l}$ where $G_{ij} \sim \mathcal{N}(0, 1)$, which provides an upper bound for the first problem in the average case. This agrees with the observation in Figure 1.

For the Gaussian random matrices, the result on the average-case stability of the partially pivoted Gaussian elimination in [3] suggests that

$$\langle \max_{ij} \left| \left(\mathbf{L}_1^{-1} \right)_{ij} \right| \rangle \lesssim l^{\frac{2}{3}}, \quad \langle \max_{ij} \left| \left(\mathbf{L}_2 \mathbf{L}_1^{-1} \right)_{ij} \right| \rangle \lesssim l^{\frac{5}{3}}.$$

Therefore, we have

$$\|\mathbf{L}_2 \mathbf{L}_1^{-1}\| \leq \|\mathbf{L}_2 \mathbf{L}_1^{-1}\|_F \leq l^{\frac{5}{3}} \sqrt{l(m-l)} = l^{\frac{13}{6}} \sqrt{m-l},$$

which implies that,

$$\eta = \left\| \begin{bmatrix} -\mathbf{I} & \mathbf{L}_2 \mathbf{L}_1^{-1} \end{bmatrix} \right\| \leq \sqrt{1 + \|\mathbf{L}_2 \mathbf{L}_1^{-1}\|^2} \lesssim l^{\frac{13}{6}} \sqrt{m-l},$$

in the average case.

C Complementary Experiments

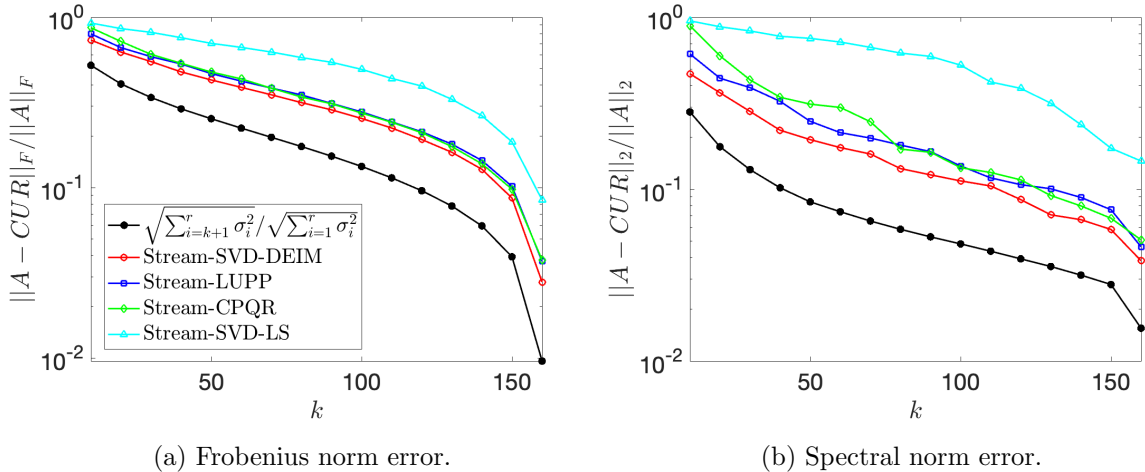


Figure 11: Relative error and runtime of the single-view CUR on the `YaleFace64x64` data set.

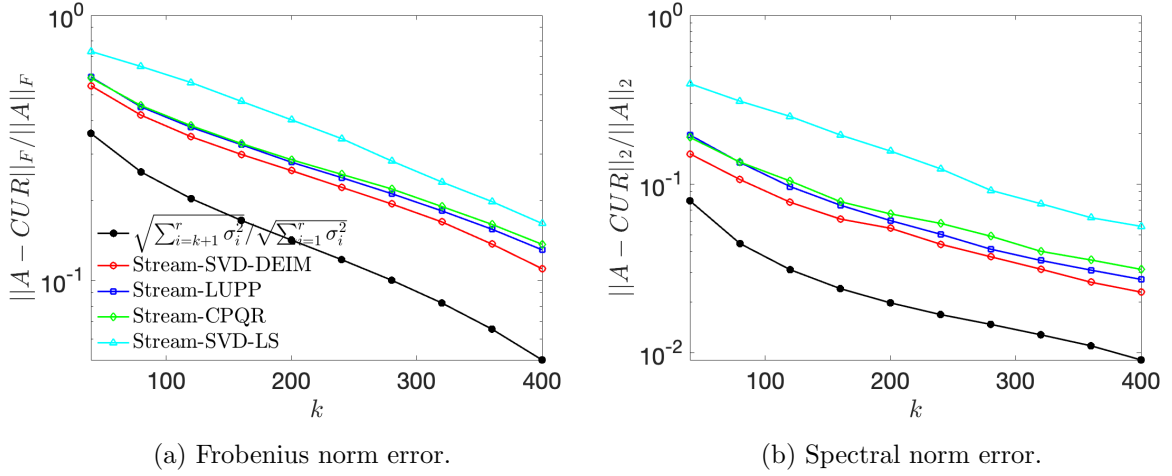


Figure 12: Relative error and runtime of the single-view CUR on the training set of MNIST.

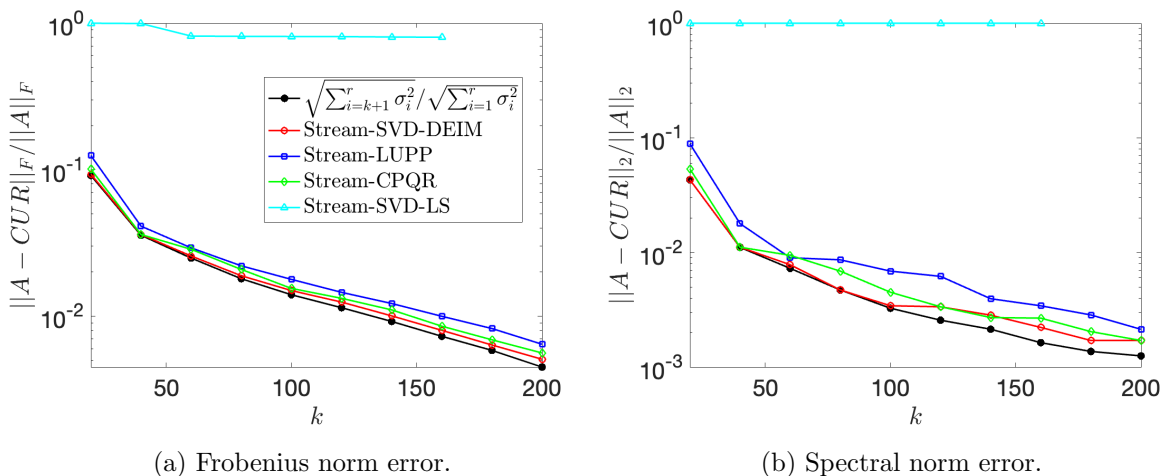


Figure 13: Relative error and runtime of the single-view CUR on a 1000×1000 sparse non-negative random matrix, SNN1e3.